Supporting Information for

Ion transport in triphenylene metal-organic columnar mesophases

Rubén Chico,[a] María Jesús Baena,[a] Cristián Cuerva,[b] Rainer Schmidt,[c] Bertrand Donnio*,[d] and Silverio Coco*,[a]*

[a] IU CINQUIMA/Química Inorgánica, Facultad de Ciencias, Universidad de Valladolid, 47011 Valladolid, Castilla y León, Spain. [b] MatMoPol, Departamento de Química Inorgánica, Facultad de Ciencias Químicas, Universidad Complutense de Madrid, Ciudad Universitaria, E-28040 Madrid, Spain. [c] GFMC, Departamento de Física de Materiales, Universidad Complutense de Madrid, Ciudad Universitaria, E-28040 Madrid, Spain. [d] Institut de Physique et Chimie des Matériaux de Strasbourg (IPCMS), CNRS-Université de Strasbourg (UMR 7504), 67034 Strasbourg, France.
* e-mail addresses: silverio.coco@uva.es, bertrand.donnio@ipcms.unistra.fr, c.cuerva@ucm.es

Table of Contents

Experimental Section

General Considerations. Elemental analyses were performed by the "Servicio de análisis elemental, CACTI, Universidad de Vigo". IR spectra were recorded on a Perkin-Elmer FT-IR SpectrumBX spectrometer. NMR spectra were recorded on Varian 500 instruments in $CDCl_3$. UV/Vis spectra were obtained by means of a Shimadzu UV-2550 spectrophotometer, in dichloromethane (~$1x10^{-4}$ M).

Luminescent data were recorded with a Perkin–Elmer LS-55 luminescence spectrometer. Luminescence quantum yields were obtained at room temperature using the optically dilute method (A < 0.1) in degassed dichloromethane (quantum yield standard was quinine sulfate dihydrate in 0.5 M H_2SO_4 (Φ_{fl} = 0.51) using an excitation wavelength of 310 nm).[1]

Mass spectra were registered at the Laboratorio de Técnicas Instrumentales (Universidad de Valladolid) by means of the MALDI-TOF technique performed in a Bruker Daltonics autoflex speed instrument equipped with nitrogen laser (340 nm). Positive ion mode spectra were recorded using the reflective mode. The accelerating voltage was 19 kV. The analytical sample was obtained by mixing the dichloromethane or tetrahydrofuran solution of the sample (1 mg/mL) and a solution of the matrix in the same solvent (DCTB, 10 mg/mL) in a 1/5 (vol/vol) ratio. The prepared solution of the sample and the matrix (0.5 μL) was loaded on the MALDI plate and allowed to dry at 23ºC before the plate was inserted into the vacuum chamber of the MALDI instrument.

Microscopy studies were carried out on a Leica DMRB microscope equipped with a Mettler FP82HT hot stage and a Mettler FP90 central processor, at a heating rate of 10 °C min^{-1}. DSC measurements were performed using a Perkin Elmer DSC-7 or a DSC Q20 from TA Instruments with samples (2−5 mg) sealed in aluminium pans and a scanning rate of 10 °C/min under a nitrogen atmosphere.

Thermogravimetric analyses (TGA) were carried out with a thermogravimetric analyser model TGA/SDTA 861 or TGA Q500 V6.7 Build 203 instrument. The samples were heated at 10 °C/min under N_2 atmosphere.

The S/WAXS patterns were obtained by transmission diffraction with a Guinier experimental set-up. A linear focalized monochromatic Cu-Kα_1 beam (λ = 1.5405 Å) was obtained using a sealed-tube generator (900 W) equipped with a bent quartz monochromator. In all cases, the crude powder was filled into thin Lindemann capillaries of 1 mm diameter and 10 μm wall thickness in air (corrections for air were made), and then heated to produce the mesophase. An initial set of diffraction patterns was recorded with a curved Inel CPS 120 counter gas-filled detector linked to a data acquisition computer; periodicities up to 70 Å can be measured, and the sample temperature controlled to within ± 0.01 ºC from 20 to 200 ºC. Alternatively, patterns were also recorded on an image plate; periodicities up to 120 Å can be measured (scanned by STORM 820 from Molecular Dynamics with 50 μm resolution). In each case, exposure times were varied from 1 to 24 h.

The ionic charge transport and dielectric properties of the compounds **1** - **4** in the solid phase, columnar mesophase and isotrope were studied by alternating current (AC) impedance spectroscopy using a Novocontrol BDS 80 AlphaT Analyzer. Measurements were performed at a frequency (*f*) range of 1 Hz to 10 MHz with six measurements points per frequency decade, using a 0.1 V amplitude for the applied AC voltage signal. The temperature (*T*) was varied between 180 K (−93 °C) and the upper limit just above the clearing temperature for each compound between of 365 - 380 K (92 - 107 °C) upon heating and cooling cycles. Dielectric data were taken under steady state conditions, i.e., the temperature was stabilized for 3−10 min before taking impedance measurements over the full *f*- range. The temperature increments/reductions for taking impedance measurements were 20−2 K steps. In particular, the temperature was increased/decreased in smaller steps near the solid-mesophase and the mesophase-isotrope phase transitions. The samples in the solid state were placed between the polished electrodes of a custom-built stainless-steel liquid cell with a high

surface to thickness ratio.[2] The cell was closed with a sapphire plate and placed inside of the Novocontrol cryostat. The dielectric response of the materials was obtained at the selected temperatures for heating and cooling cycles in terms of the real and imaginary parts (Z′, Z″) of the complex impedance Z* = Z′ + iZ″. The data were converted into the complex conductivity σ* and capacitance C* notations, σ* = σ′ + iσ″ and C* = C′ − iC″, using the standard conversions: $Z^* = (g\sigma^*)^{-1}$, and $Z^* = (i\omega C^*)^{-1}$, where g (in cm) is the geometrical factor given by electrode area divided by electrode distance and ω is the angular frequency. The geometrical factor g could only be estimated from the weight and density of the powder measured initially and the dimensions of the liquid cell. Equivalent circuit fitting of the dielectric data was performed by using Z-View software and a custom-built automated data analysis tool based on two advanced Microsoft Excel macros.

Synthesis. Literature methods were used for the synthesis of 2-(6–(4-isocyanophenoxy)hexyloxy)-3,6,7,10,11-penta(dodecyloxy)triphenylene ($CNC_6H_4OC_6H_{12}O$-TPh),[3] and [AuCl(tht)].[4] Commercial reagents and reagent grade solvents were used as purchased.

Preparation of $[Ag(CNC_6H_4OC_6H_{12}O\text{-}TPh)_2]NO_3$ (1). A solution of $CNC_6H_4OC_6H_{12}O$-TPh (97.0 mg, 0.071 mmol) in 20 mL of THF was added to a suspension of $AgNO_3$ (6.2 mg, 0.035 mmol) in 10 mL of acetone. The mixture was protected from the light and stirred for 2 hours. After evaporation of the solvents, the residue was recrystallized from CH_2Cl_2/Et_2O to afford the product as a light-yellow solid, which was dried under vacuum at 60 °C for 20 min. Yield: 75.1 mg, 73 %. IR (CH_2Cl_2/cm^{-1}) ν(C≡N): 2189, (KBr): 2191. Elemental analysis: calculated (%) for $C_{182}H_{294}N_3AgO_{17}$: C, 75.27; H, 10.20; N, 1.45; found: C, 74.99; H, 9.92; N, 1.31. ^{1}H NMR ($CDCl_3$, 500 MHz): δ 7.84 (s, 12H, H_{TPh}), 7.39 (d, 4H[1], $H_{ar,}$ AA' part of AA'XX' spin system, $N_{1,2} = J_{1,2} + J_{1,2'} = 8.8$ Hz, $J_{1,1'} \approx J_{2,2'}$), 6.89 (d, 4H[2], H_{ar}, XX' part of AA'XX'spin system AA'XX' ($N_{1,2} = J_{1,2} + J_{1,2'} = 8.8$ Hz, $J_{1,1'} \approx J_{2,2'}$), 4.23 (m, 24H, OCH_2), 4.01 (t, 4H, $J = 6.4$ Hz, OCH_2), 2.04 – 1.80 (m, 28H, OCH_2CH_2), 1.75-1.20 (m, 188H, CH_2), 0.88 (m, 30H, CH_3). $^{13}C\{^1H\}$ NMR (126 MHz, $CDCl_3$,

Me_4Si): δ 160.90 (O-**C$_{ar}$**), 149.07 (N-**C$_{ar}$**), 149.04, 148.99, 148.94, 148.92, 148.79 (O-**C$_{TPh}$**), 128.49 (H-**C$_{ar}$**), 125.49, 123.70, 123.65, 123.55 (**C$_{TPh}$**), 115.37 (H-**C$_{ar}$**), 107.56, 107.39, 107.18 (H-**C$_{TPh}$**), 69.84, 69.74, 69.69, 69.57, 69.42, 68.45 (O-**CH$_2$**), 31.93, 29.73, 29.71, 29.68, 29.55, 29.49, 29.38, 26.22, 25.92, 25.78, 22.69 (-**CH$_2$**-), 14.11(-**CH$_3$**). MALDI-TOF: positive m/z calcd. for $C_{91}H_{148}AgNO_7$ $[M - CNR - NO_3 + H]^+$: 1474.0, found: 1473.9; calcd. for $C_{91}H_{147}NO_7$ $[CNR]^+$: 1366.1, found: 1366.0; negative m/z calcd. for NO_3^-: 62.0, found: 62.1.

Preparation of [Ag(CNC$_6$H$_4$OC$_6$H$_{12}$O-TPh)$_2$]BF$_4$ (2). Compound **2** was prepared following the same method as for complex **1** but using $AgBF_4$. Starting products: $CNC_6H_4OC_6H_{12}O$-TPh (104.5 mg, 0.076 mmol) and $AgBF_4$ (7.5 mg, 0.038 mmol). Yield: 87.4 mg, 78 %. IR (CH_2Cl_2/cm^{-1}) ν(C≡N): 2209, (KBr): 2192. Elemental analysis: calculated (%) for $C_{182}H_{294}N_2AgBF_4O_{14}$: C, 74.63; H, 10.12; N, 0.96; found: C, 74.32; H, 9.71; N, 0.98. ^{1}H NMR ($CDCl_3$, 500 MHz): δ 7.84 (s, 12H, H_{TPh}), 7.48 (d, 4H^1, $H_{ar,}$ AA' part of AA'XX' spin system, $N_{1,2} = J_{1,2} + J_{1,2'} = 9.1$ Hz, $J_{1,1'} \approx J_{2,2'}$), 6.92 (d, 4H^2, H_{ar}, XX' part of AA'XX' spin system, $N_{1,2} = J_{1,2} + J_{1,2'} = 9.1$ Hz, $J_{1,1'} \approx J_{2,2'}$) 4.23 (m, 24H, OCH_2), 4.01 (t, 4H, J = 6.4 Hz, OCH_2), 2.00 – 1.80 (m, 28H, OCH_2CH_2), 1.75-1.20 (m, 188H, CH_2), 0.88 (m, 30H, CH_3). ^{13}C{^{1}H} NMR (126 MHz, $CDCl_3$, Me_4Si): δ 160.67 (O-**C$_{ar}$**), 149.09 (N-**C$_{ar}$**), 149.05, 149.03, 149.00, 148.98, 148.95, 148.84 (O-**C$_{TPh}$**), 128.51 (H-**C$_{ar}$**), 123.71, 123.67, 123.65, 123.58 (**C$_{TPh}$**), 115.33 (H-**C$_{ar}$**), 107.45, 107.41, 107.37 (H-**C$_{TPh}$**), 69.81, 69.74, 69.71, 69.61, 69.48, 68.44 (O-**CH$_2$**), 31.92, 29.73, 29.70, 29.67, 29.54, 29.51, 29.37, 26.21, 25.98, 25.85, 22.68 (-**CH$_2$**-), 14.11(-**CH$_3$**). ^{19}F NMR (470 MHz, $CDCl_3$) δ –150,76 BF_4^-). MALDI-TOF: positive m/z calcd. for $C_{91}H_{148}AgNO_7$ $[M - CNR - BF_4 + H]^+$: 1474.0, found: 1473.9; calcd. for $C_{91}H_{147}NO_7$ $[CNR]^+$: 1366.1, found: 1366.0; negative m/z calcd. for BF_4^-: 87.0; found: 87.0.

Preparation of [Au(CNC$_6$H$_4$OC$_6$H$_{12}$O-TPh)$_2$]NO$_3$ (3): **[**AuCl(tht)] (10.1 mg, 0.031 mmol) was dissolved in 25 mL THF and introduced in a bath at -40ºC. Under constant stirring, tht (3 mg, 0.034 mmol) and $AgNO_3$ (5.5 mg, 0.032 mmol) were added. The reaction mixture was then slowly brought to -10ºC (1 h). The generated white precipitate of AgCl was filtered off and the filtrate collected

over a solution of $CNC_6H_4OC_6H_{12}O$-TPh (86.1 mg, 0.063 mmol) in THF (10 mL) at 0ºC. After stirring for 1 hour at 0ºC, evaporation of the solvent afforded a light-yellow solid. Yield: 63.2 mg, 67 %. IR (CH_2Cl_2/cm^{-1}) ν(C≡N): 2226, (KBr): 2224. Elemental analysis (%) for $C_{182}H_{294}N_3AuO_{17}$: calculated: C, 73.03; H, 9.90; N, 1.40; found: C, 73.29; H, 9.78; N, 1.52. ^{1}H NMR ($CDCl_3$, 500 MHz): δ 7.84 (m, 12H, H_{Tp}), 7.32 (m, 4H^1, H_{ar}, AA' part of AA'XX' spin system, $N_{1,2} = J_{1,2} + J_{1,2'}$= 8.7 Hz, $J_{1,1'} \approx J_{2,2'}$), 6.87 (m, 4H^2, H_{ar}, XX' part of AA'XX' spin system, $N_{1,2} = J_{1,2} + J_{1,2'}$= 8.7 Hz, $J_{1,1'} \approx J_{2,2'}$), 4.23 (m, 24H, OCH_2), 4.00 (m, 4H, OCH_2), 2.09 - 1.80 (m, 28H, OCH_2CH_2), 1.75 - 1.20 (m, 188H, CH_2), 0.88 (m, 30H, CH_3). $^{13}C\{^1H\}$ NMR (126 MHz, $CDCl_3$, Me_4Si): δ 160.97 (O-**C$_{ar}$**), 149.12 (N-**C$_{ar}$**), 149.00, 148.90, 148.74, (O-**C$_{TPh}$**), 128.31 (H-**C$_{ar}$**), 125.51, 123.67, 123.51, 123.47 (**C$_{TPh}$**), 115.47 (H-**C$_{ar}$**), 107.65, 107.38, 107.14 (H-**C$_{TPh}$**), 69.91, 69.81, 69.72, 69.65, 69.56, 68.43 (O-**CH$_2$**), 31.93, 29.73, 29.71, 29.68, 29.55, 29.49, 29.38, 26.22, 25.79, 25.62, 22.69 (-**CH$_2$**-), 14.11 (-**CH$_3$**). MALDI-TOF: positive m/z calcd. for $C_{182}H_{294}AuN_2O_{14}$ $[M - NO_3]^+$: 2929.2, found: 2929.3; negative m/z calcd. for NO_3^-: 62.10, found: 61.98.

Preparation of [Au($CNC_6H_4OC_6H_{12}O$-TPh)$_2$]BF_4 (4): Compound **4** was prepared following the same method as for complex **3** but using $AuBF_4$. Starting products: [AuCl(tht)] (11.5 mg, 0.036 mmol), tht (4 mg, 0.045 mmol), $AgBF_4$ (7.0 mg, 0.036 mmol), $CNC_6H_4OC_6H_{12}O$-TPh (98.1 mg, 0.072 mmol). Yield: 71.1 mg, 66%. IR (CH_2Cl_2/cm^{-1}) ν(C≡N): 2232, (KBr): 2230. Elemental analysis (%) for $C_{185}H_{297}AuBF_4N_2O_{14}$: calculated: C, 72.47.; H, 9.87; N, 0.92; found: C, 72.42; H, 9.24; N, 0.94. ^{1}H NMR ($CDCl_3$, 500 MHz): δ 7.83 (m, 12H, H_{Tp}), 7.47 (d, 4H^1, H_{ar}, AA' part of AA'XX' spin system, $N_{1,2} = J_{1,2} + J_{1,2'}$= 8.5 Hz, $J_{1,1'} \approx J_{2,2'}$), 6.91 (d, 4H^2, H_{ar}, XX' part of AA'XX' spin system, $N_{1,2} = J_{1,2} + J_{1,2'}$= 8.5 Hz, $J_{1,1'} \approx J_{2,2'}$), 4.24 (m, 24H, OCH_2), 4.03 (t, 4H, J = 6.5 Hz, OCH_2), 2.01 – 1.80 (m, 28H, OCH_2CH_2), 1.75 – 1.20 (m, 188H, CH_2), 0.88 (m, 30H, CH_3). $^{13}C\{^1H\}$ NMR (126 MHz, $CDCl_3$, Me_4Si): δ 149.09 (N-**C$_{ar}$**), 149.03, 148.80 (O-**C$_{TPh}$**), 129.31 (H-**C$_{ar}$**), 123.69, 123.65, 123.55, 123.53 (**C$_{TPh}$**), 115.61 (H-**C$_{ar}$**), 107.39, 107.34, 107.31 (H-**C$_{TPh}$**), 69.88,

69.75, 69.71, 69.58, 69.23, 68.55 (O-**CH_2**), 31.93, 30.31, 29.71, 29.68, 29.54, 29.51, 29.38, 26.22, 25.76, 25.60, 22.69 (-**CH_2**-), 14.12(-**CH_3**). ^{19}F NMR (470 MHz, $CDCl_3$) δ 150,76 (BF_4^-). MALDI-TOF: positive m/z calcd. for $C_{182}H_{294}AuN_2O_{14}$ $[M - BF_4]^+$: 2929.2015, found: 2929.2031; negative m/z calcd. for BF_4^-: 87.0; found: 87.1.

^{1}H NMR spectra ($CDCl_3$, 400 MHz)

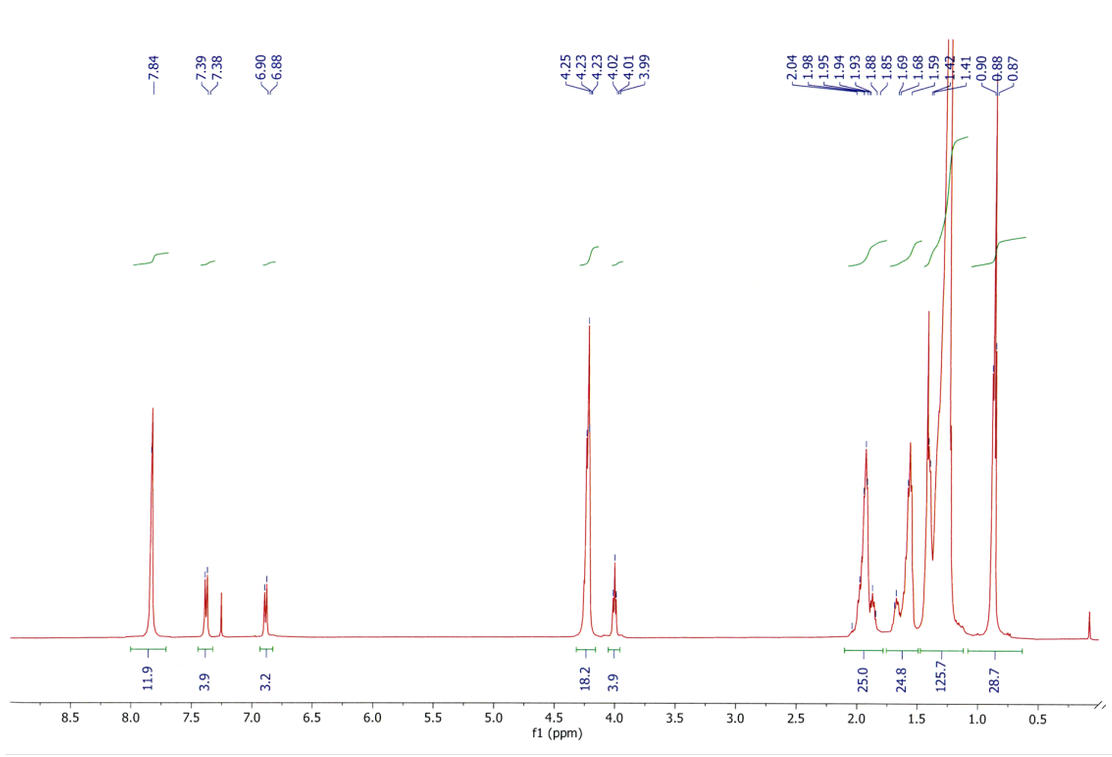

Figure S1. ^{1}H NMR spectrum of **1.**

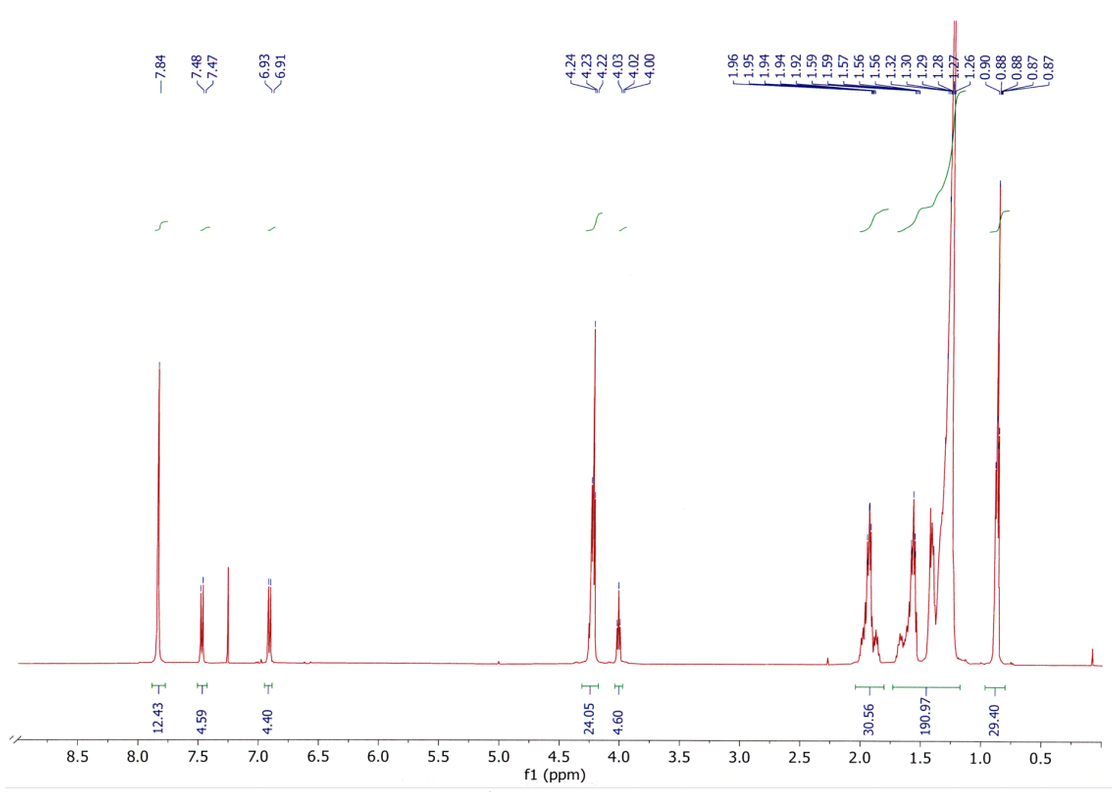

Figure S2. ^{1}H NMR spectrum of **2.**

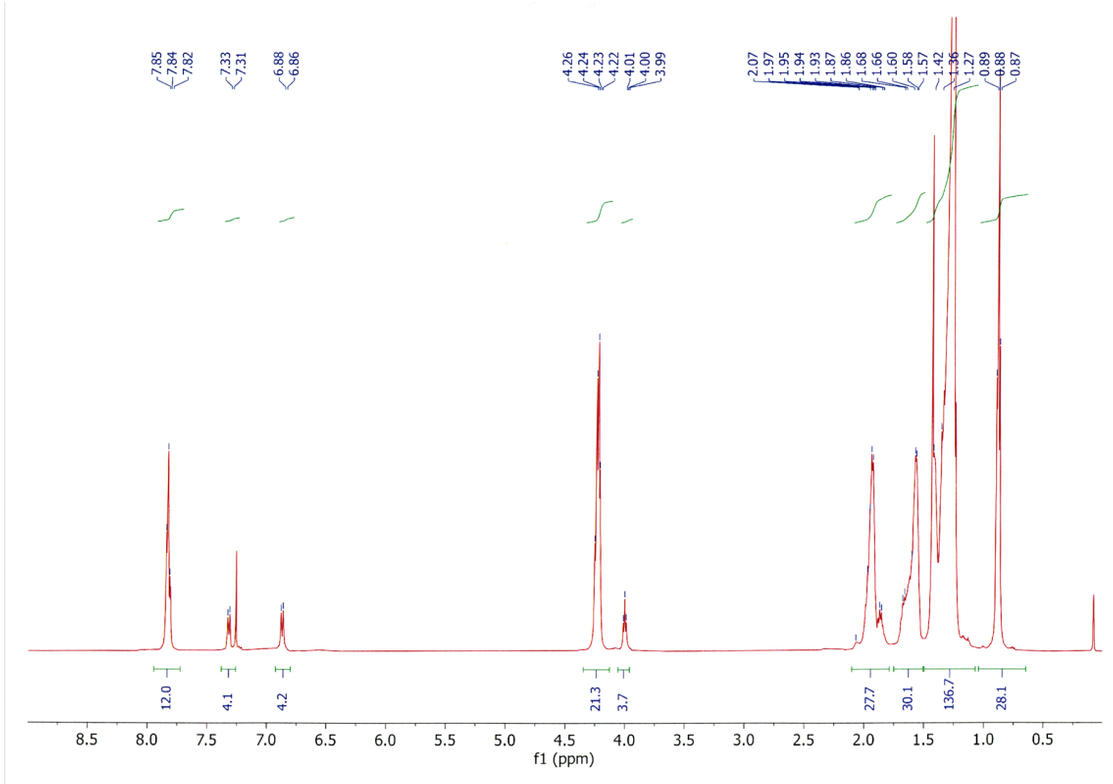

Figure S3. ^{1}H NMR spectrum of **3**.

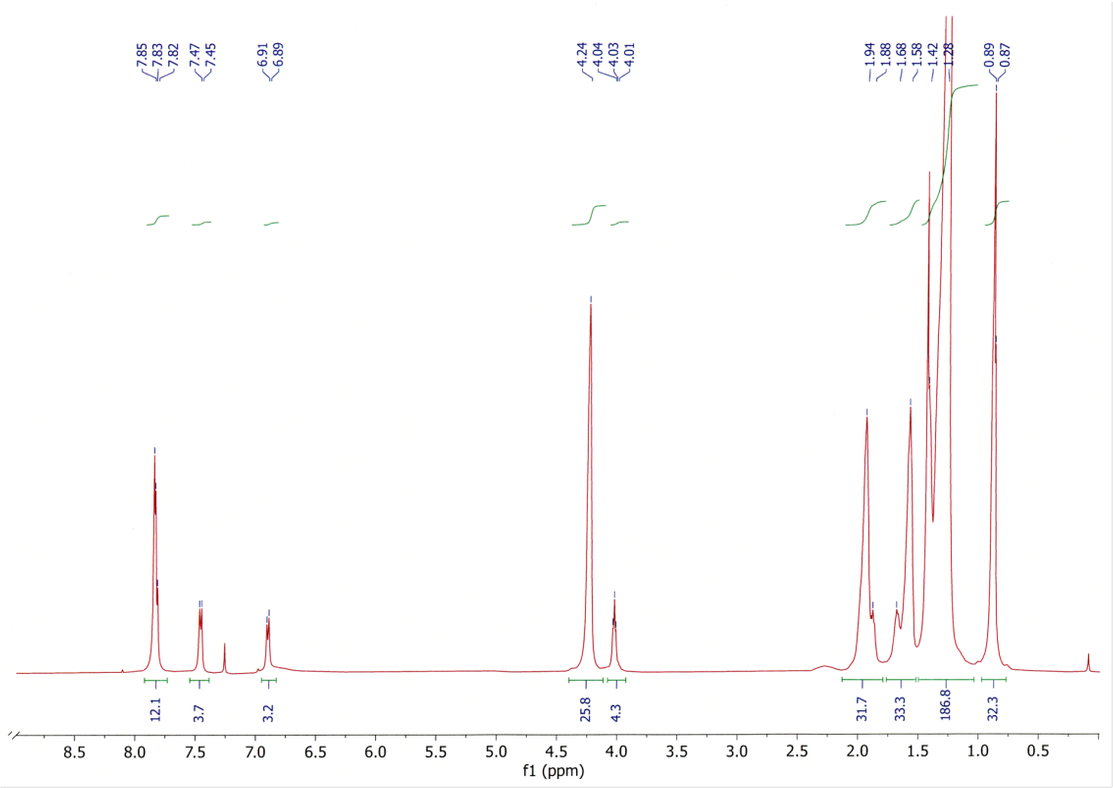

Figure S4: ^{1}H NMR spectrum of **4**.

$^{13}C\{^{1}H\}$ NMR spectra (Agilent 500 (126 MHz) in $CDCl_3$

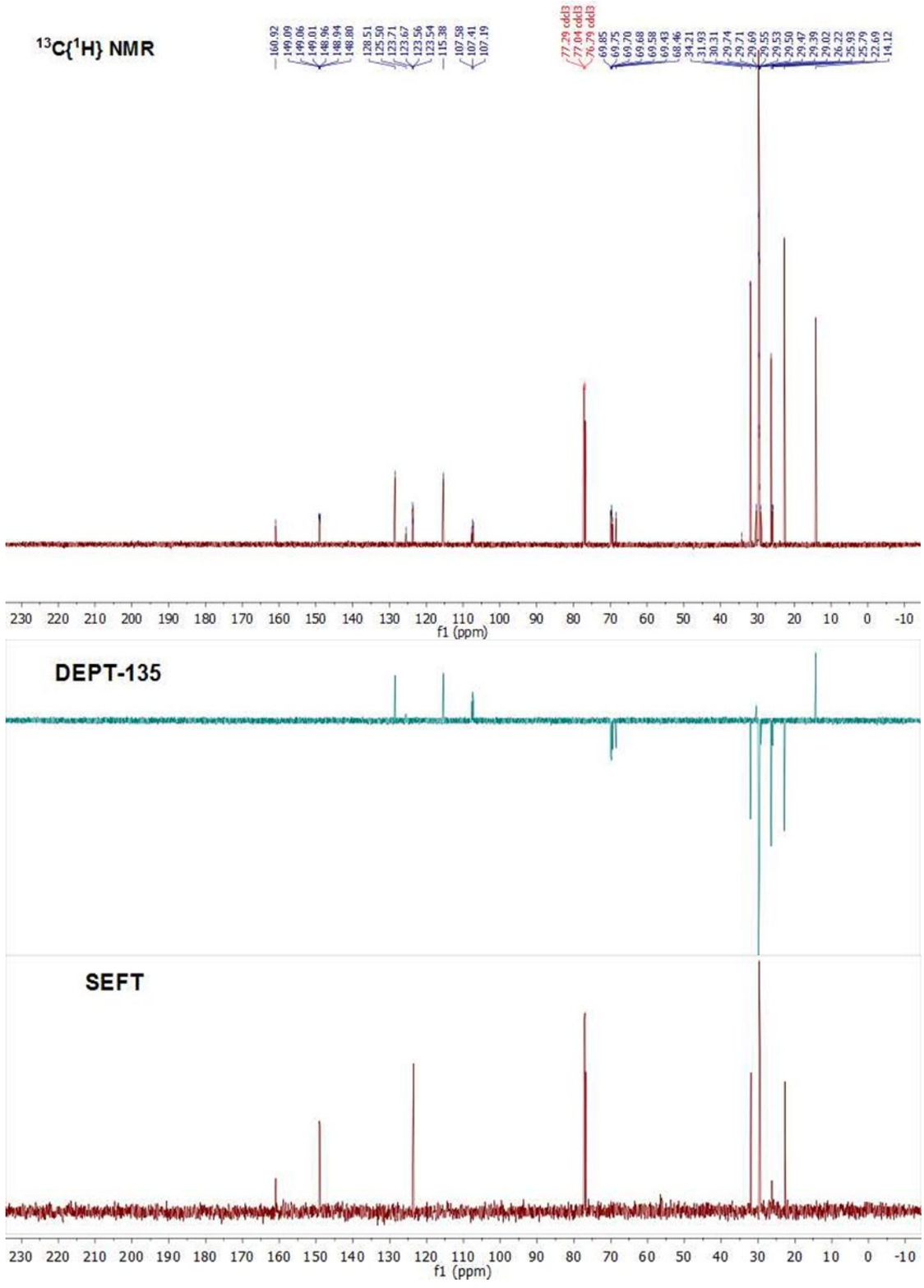

Figure S5. $^{13}C\{^{1}H\}$ NMR spectra of **1**

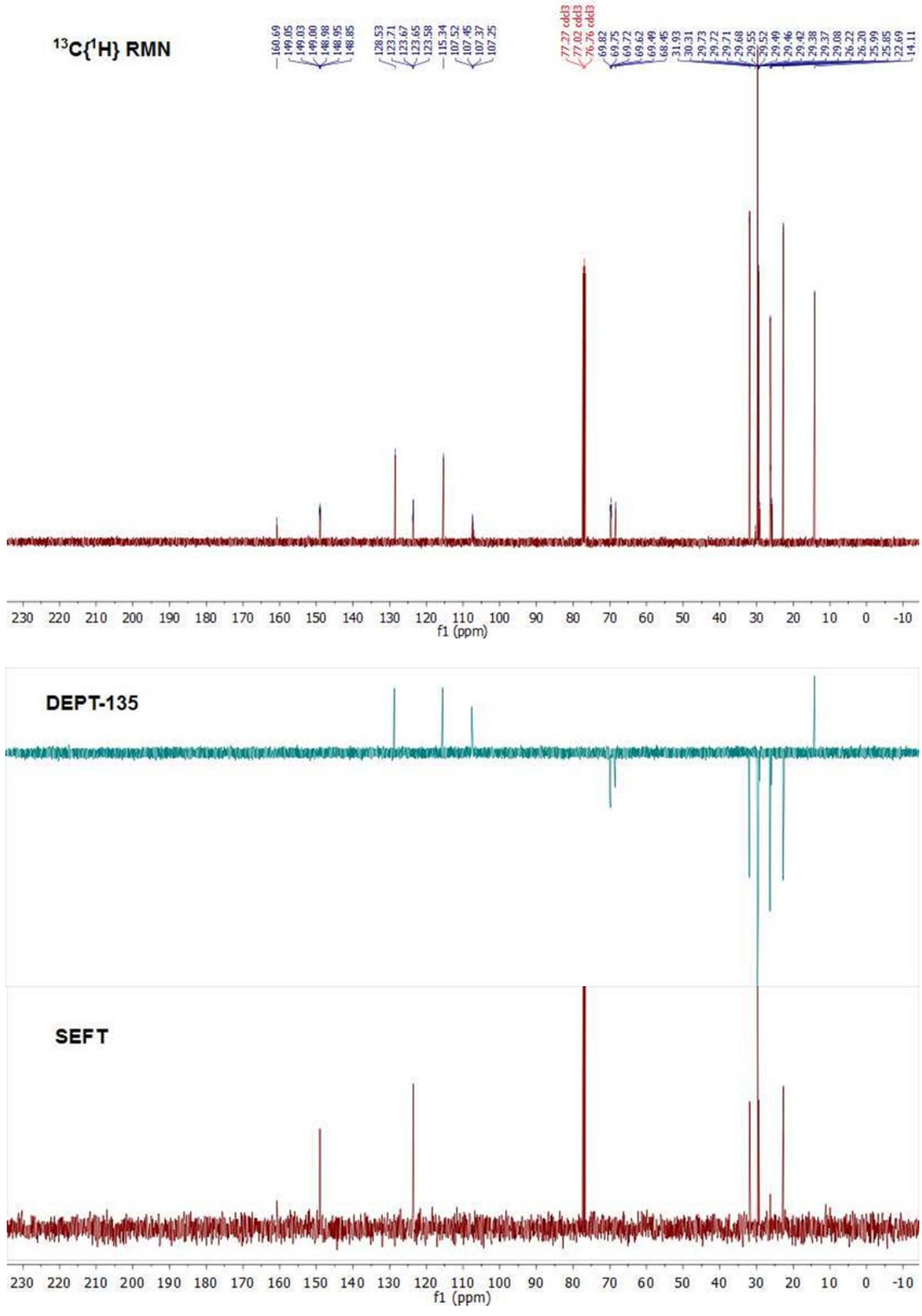

Figure S6. $^{13}C\{^{1}H\}$ NMR spectra of **2**

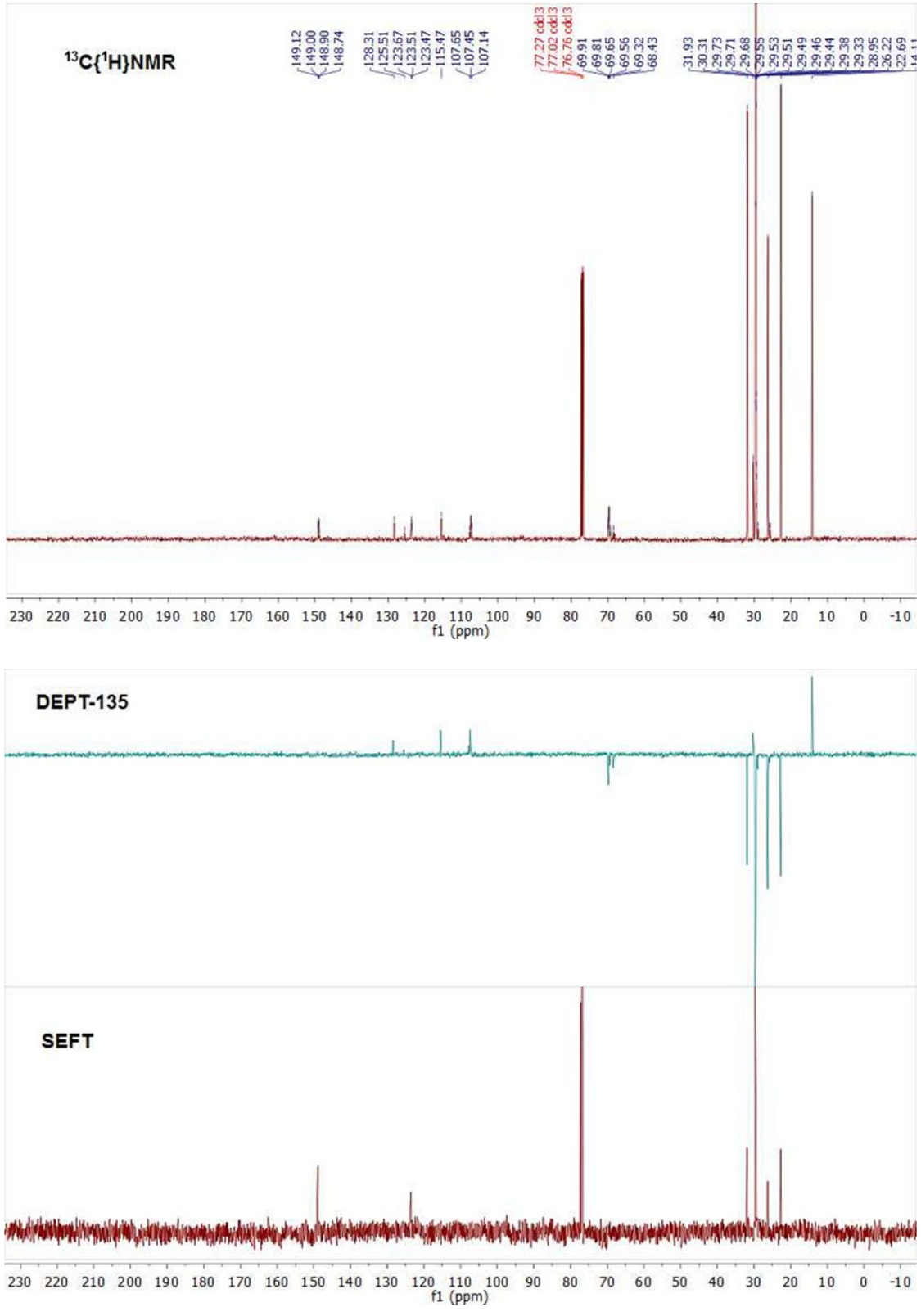

Figure S7. $^{13}C\{^{1}H\}$ NMR spectra of **3.**

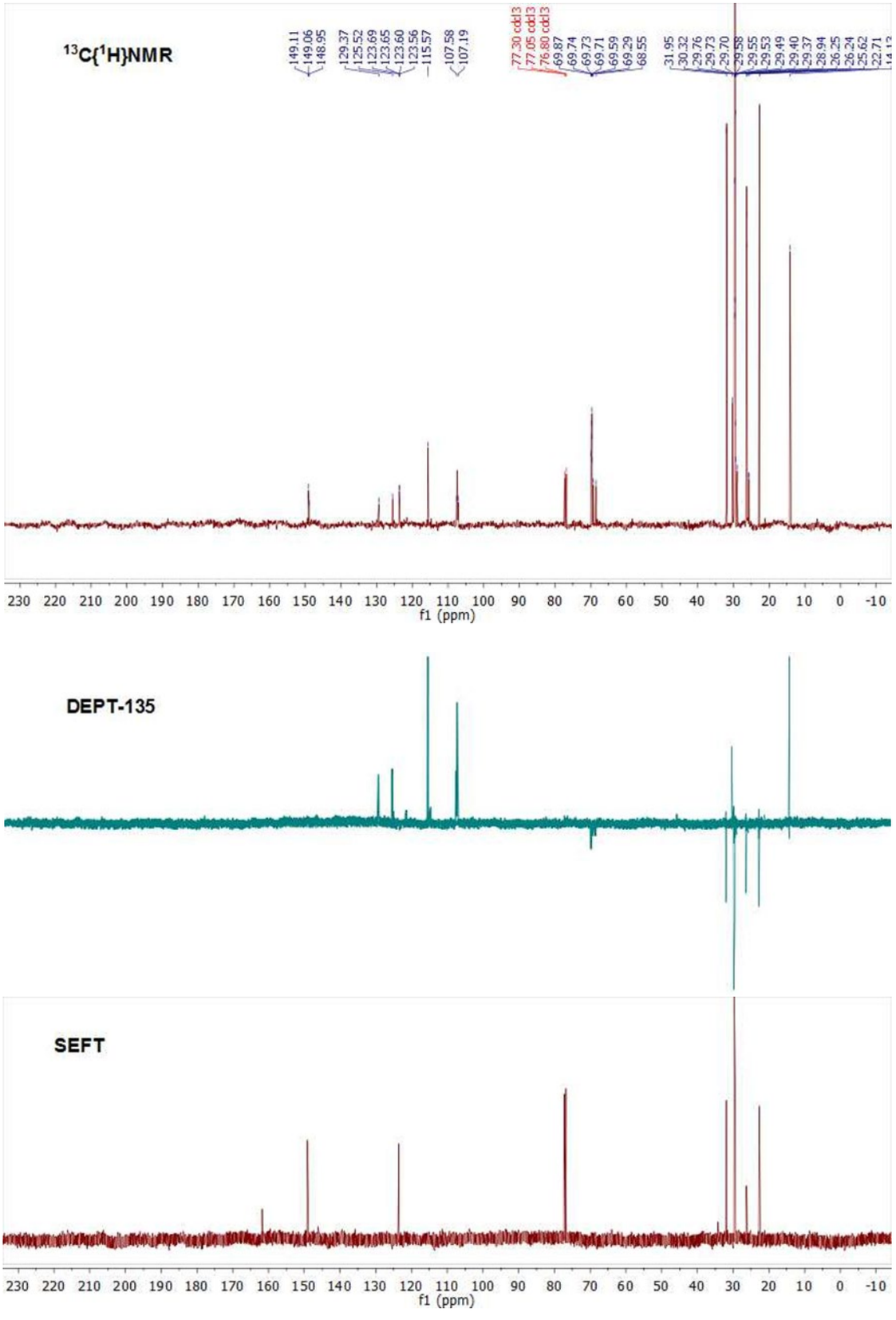

Figure S8. $^{13}C\{^{1}H\}$ NMR spectra of **4**

^{19}F NMR spectra (Agilent 500 (470 MHz) in $CDCl_3$

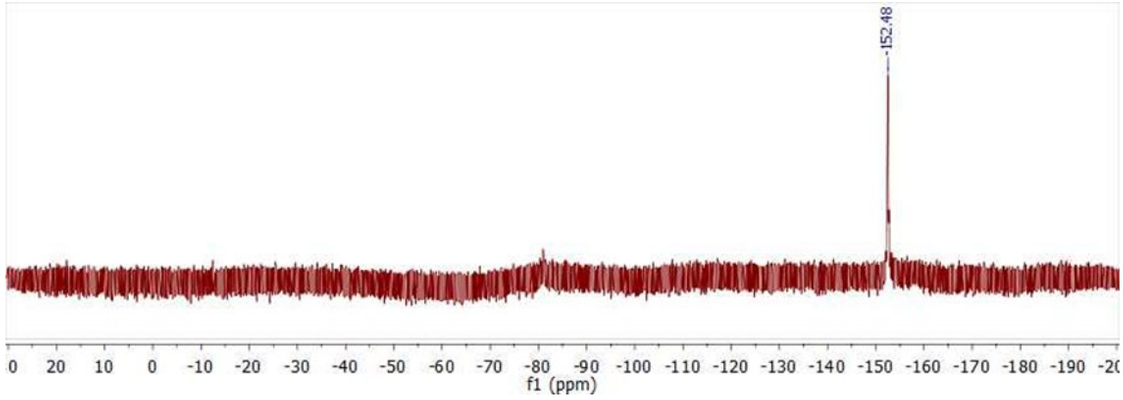

Figure S9. ^{19}F NMR spectrum of **2**

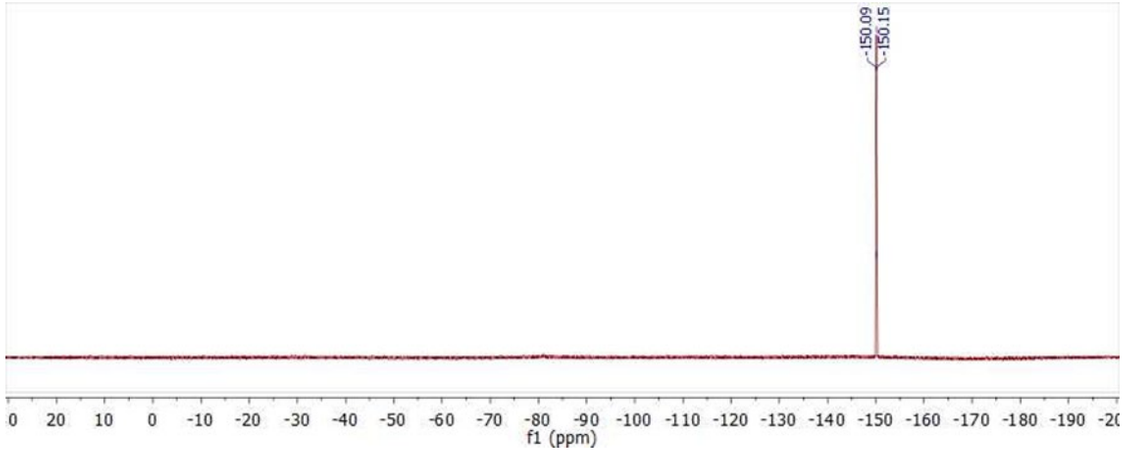

Figure S10. ^{19}F NMR spectrum of **4**

MALDI-TOF mass spectra

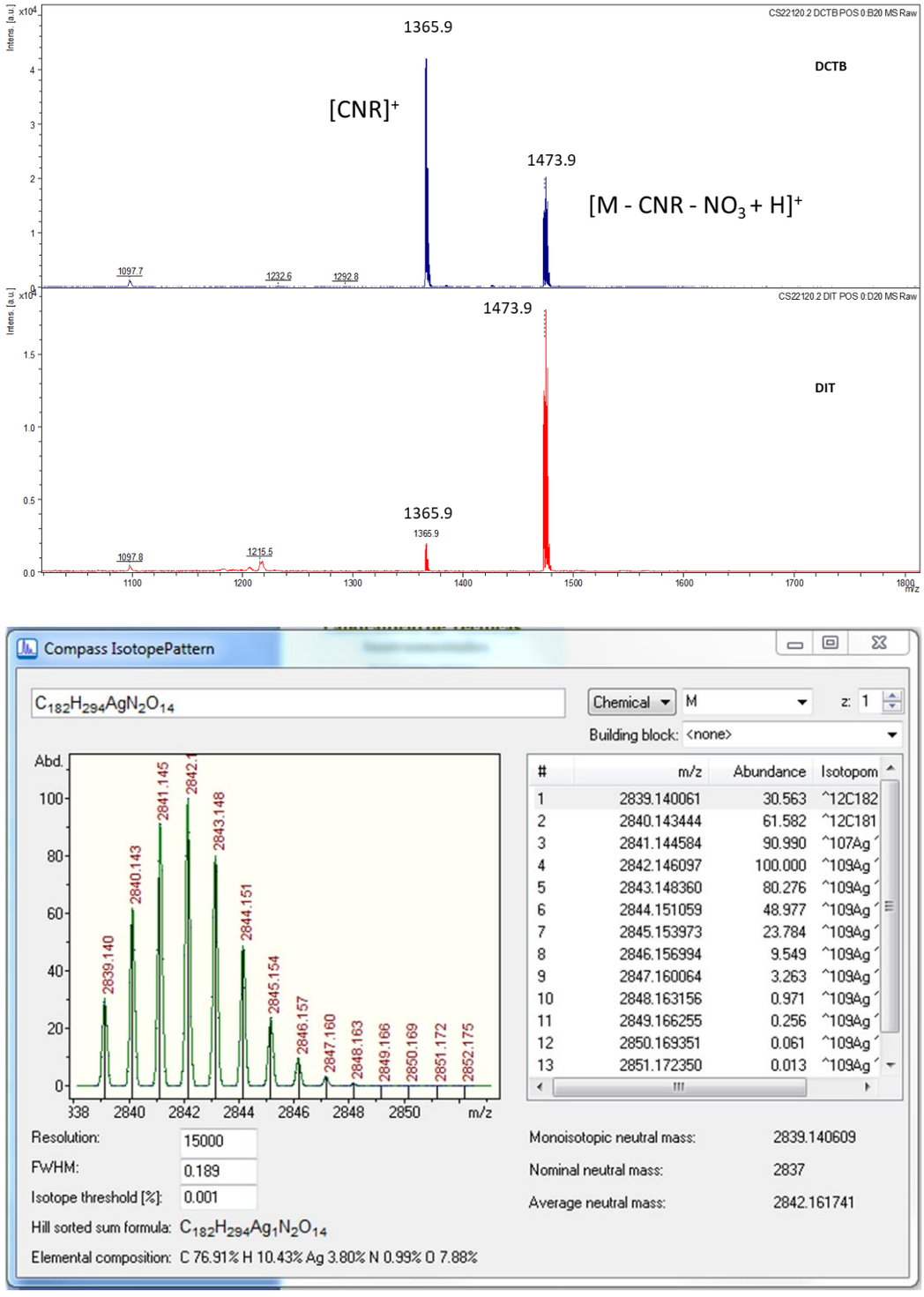

Figure S11. Up, MALDI-TOF (positive m/z) spectrum of **1**. Red with DIT (dithranol) as matrix; Blue with DCTB (trans-2-[3-(4-tert-Butylphenyl)-2-methyl-2-propenylidene]malononitrile) as matrix. Down, simulated isotopic pattern for $[M - NO_3]^+$.

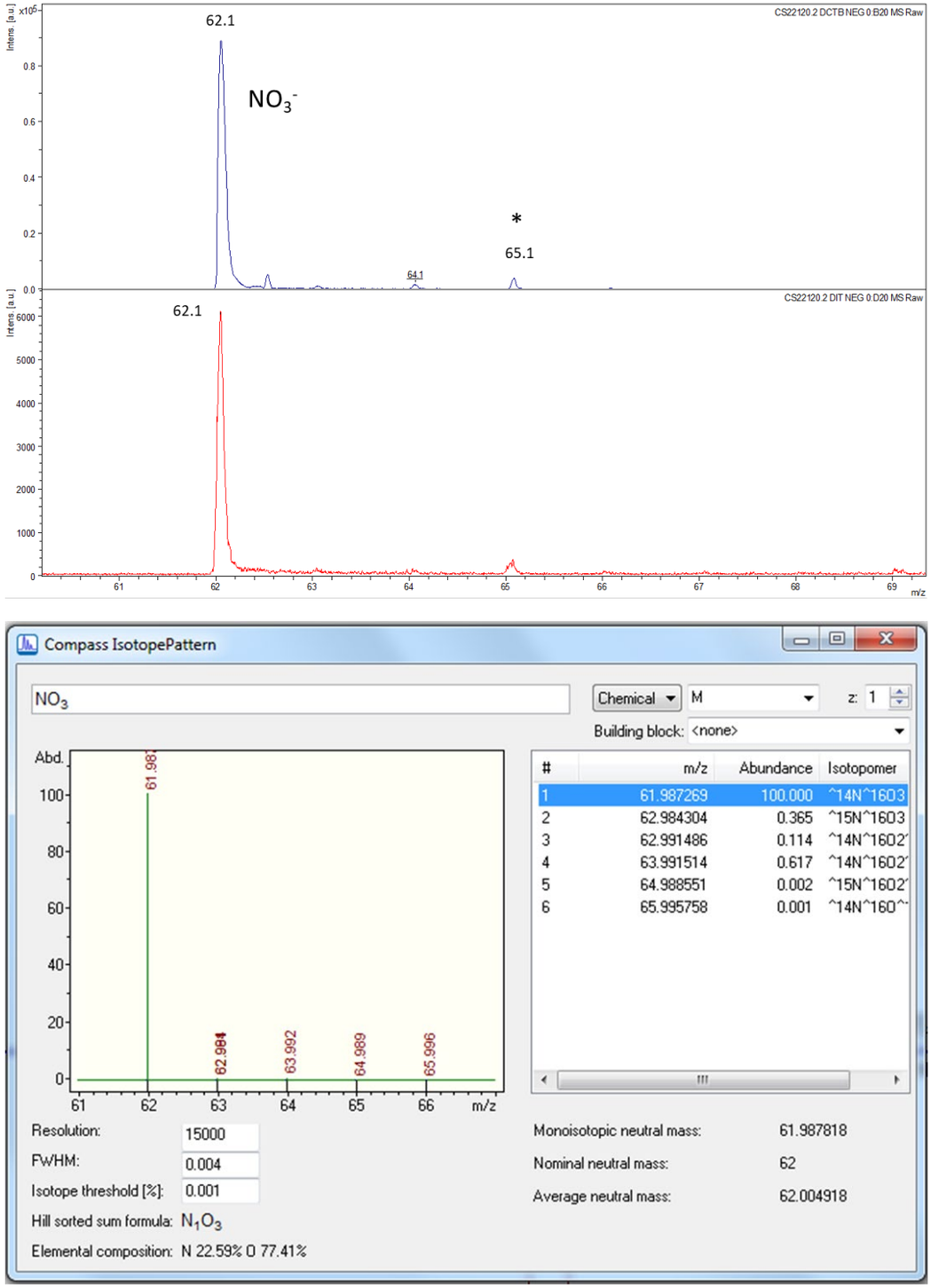

Figure S12. Up, MALDI-TOF (negative m/z) spectrum of compound **1**. Red with DIT (dithranol) as matrix; Blue with DCTB (trans-2-[3-(4-tert-Butylphenyl)-2-methyl-2-propenylidene]malononitrile) as matrix. * Peak from the matrix. Down, simulated isotopic pattern for NO_3^-.

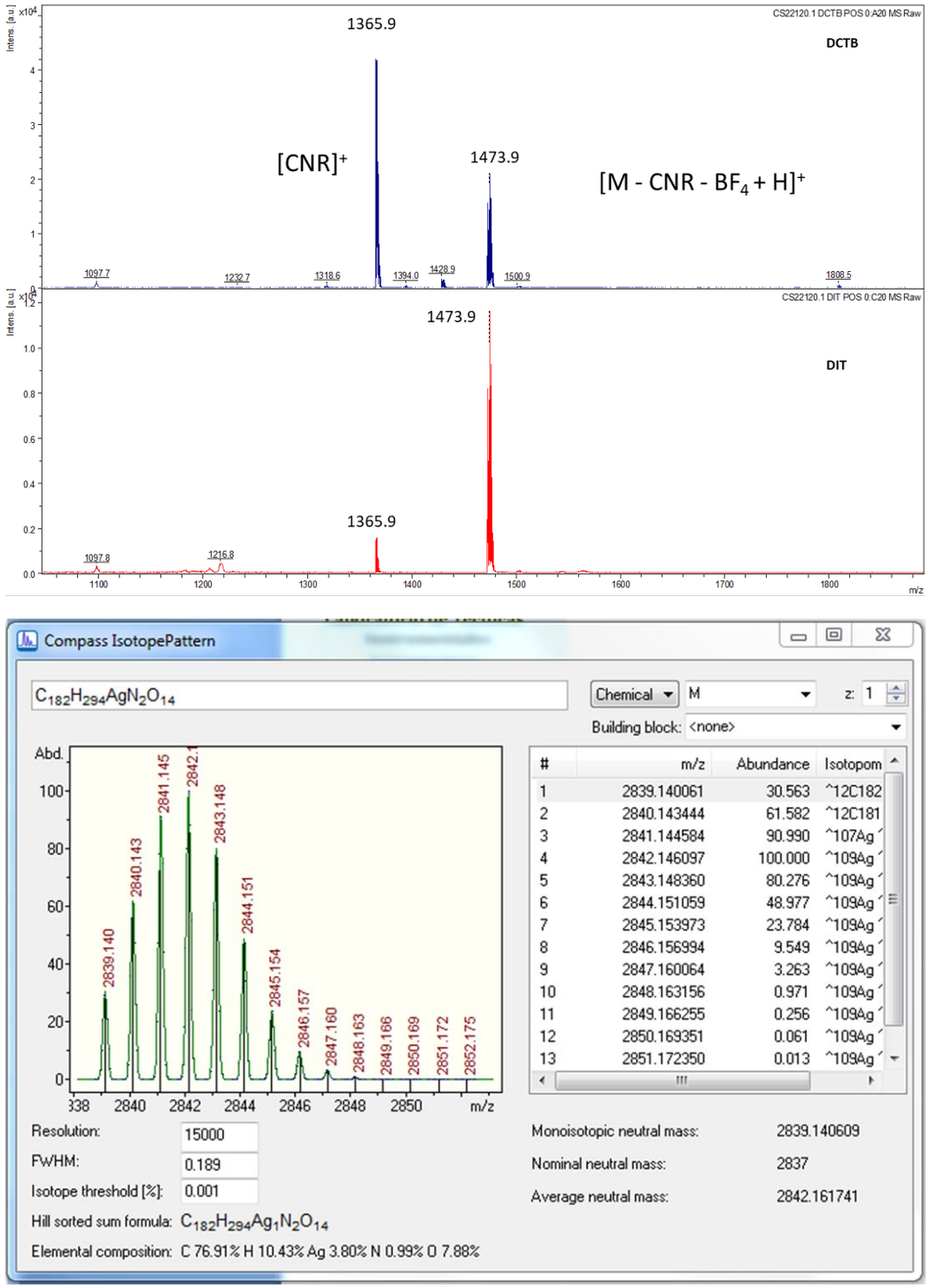

Figure S13. Up, MALDI-TOF (positive m/z) spectrum of **2**. Red with DIT (dithranol) as matrix; Blue with DCTB (trans-2-[3-(4-tert-Butylphenyl)-2-methyl-2-propenylidene]malononitrile) as matrix. Down, simulated isotopic pattern for $[M - BF_4]^+$.

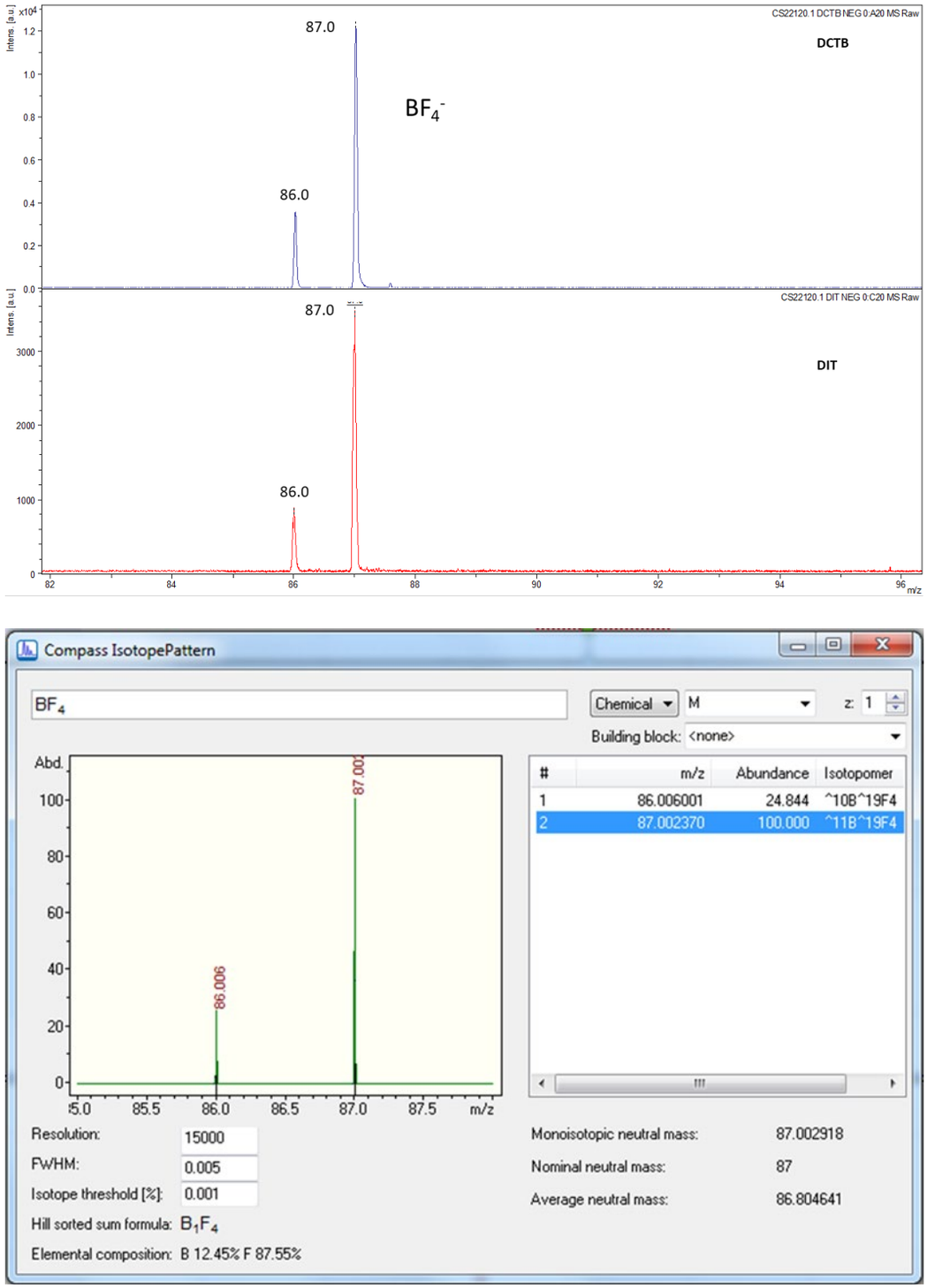

Figure S14. Up, MALDI-TOF (negative m/z) spectrum of **2**. Red with DIT (dithranol) as matrix; Blue with DCTB (trans-2-[3-(4-tert-Butylphenyl)-2-methyl-2-propenylidene]malononitrile) as matrix. Down, simulated isotopic pattern for BF_4^-.

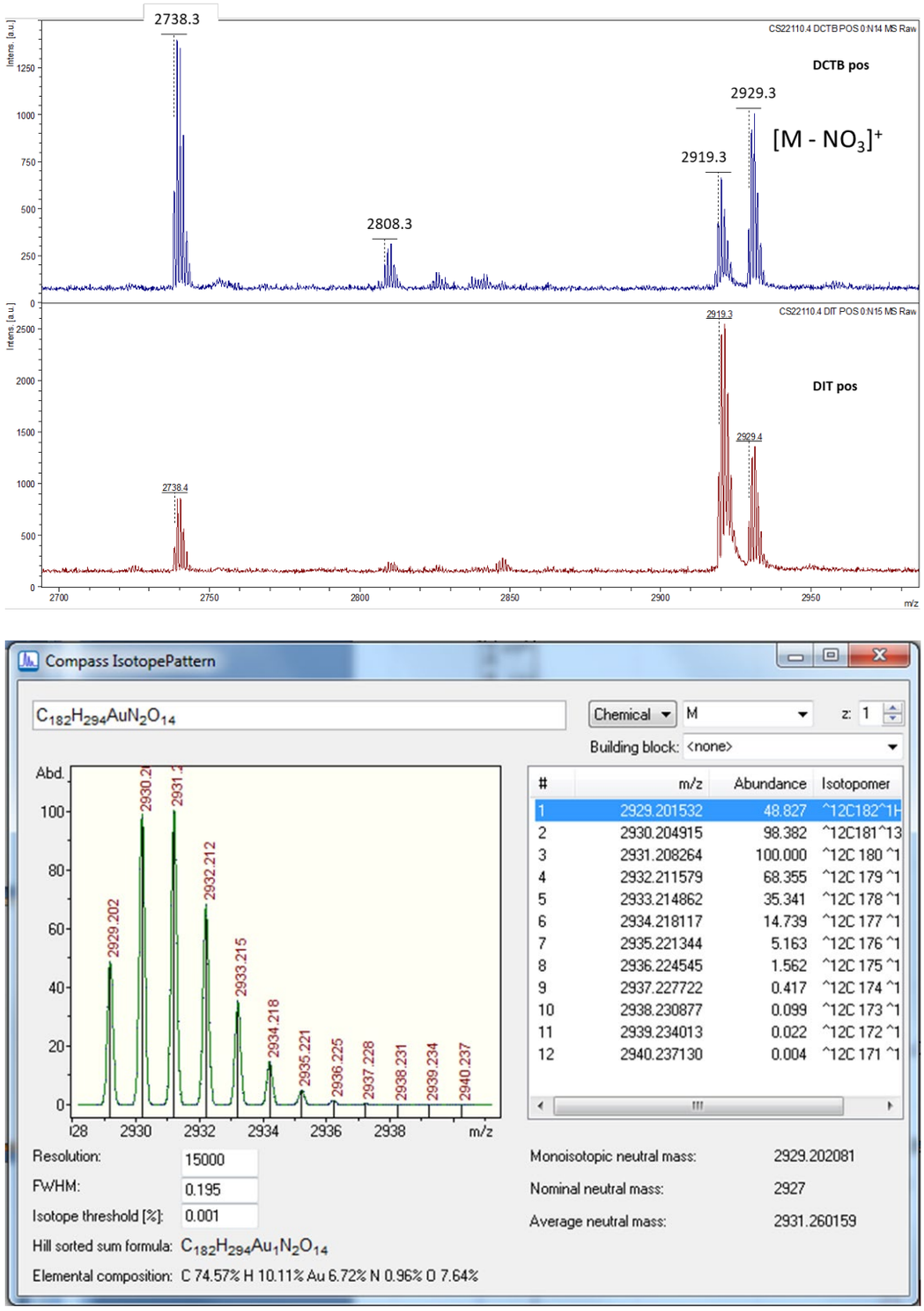

#	m/z	Abundance	Isotopomer
1	2929.201532	48.827	^12C182^1H
2	2930.204915	98.382	^12C181^13
3	2931.208264	100.000	^12C 180 ^1
4	2932.211579	68.355	^12C 179 ^1
5	2933.214862	35.341	^12C 178 ^1
6	2934.218117	14.739	^12C 177 ^1
7	2935.221344	5.163	^12C 176 ^1
8	2936.224545	1.562	^12C 175 ^1
9	2937.227722	0.417	^12C 174 ^1
10	2938.230877	0.099	^12C 173 ^1
11	2939.234013	0.022	^12C 172 ^1
12	2940.237130	0.004	^12C 171 ^1

Figure S15. Up, MALDI-TOF (positive m/z) spectrum of compound **3**. Red with DIT (dithranol) as matrix; Blue with DCTB (trans-2-[3-(4-tert-Butylphenyl)-2-methyl-2-propenylidene]malononitrile) as matrix. Down, simulated isotopic pattern for $[M - NO_3]^+$.

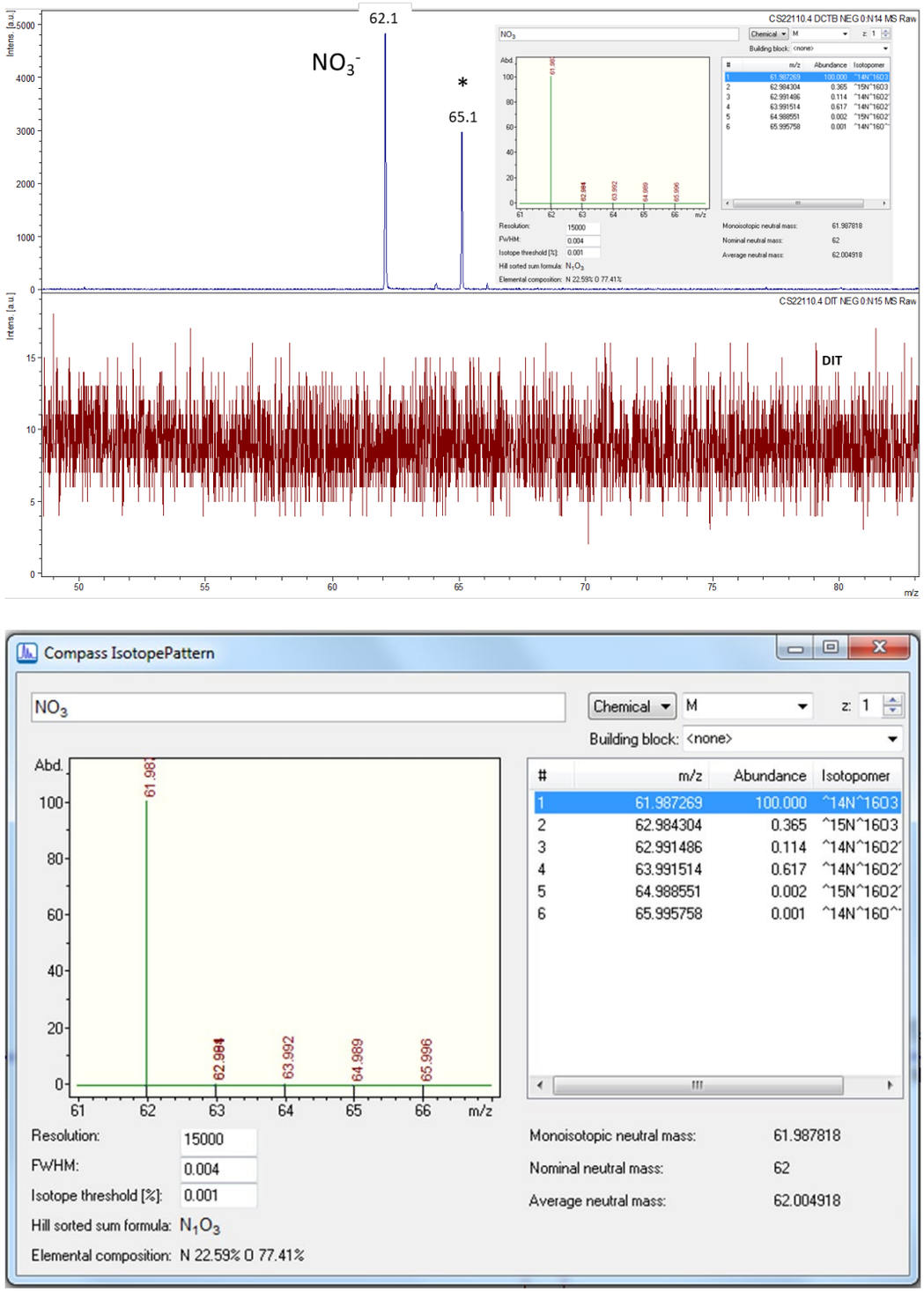

Figure S16. Up, MALDI-TOF (negative m/z) spectrum of compound **3**. Red with DIT (dithranol) as matrix; Blue with DCTB (trans-2-[3-(4-tert-Butylphenyl)-2-methyl-2-propenylidene]malononitrile) as matrix. * Peak from the matrix. Down, simulated isotopic pattern for NO_3^-. Down, simulated isotopic pattern for NO_3^-.

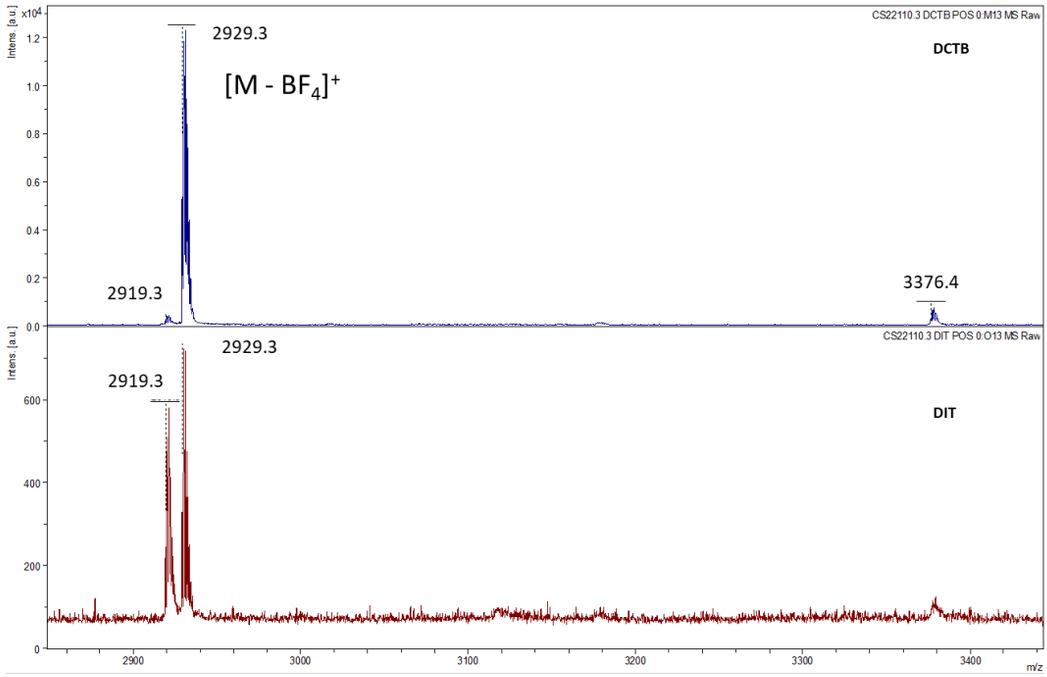

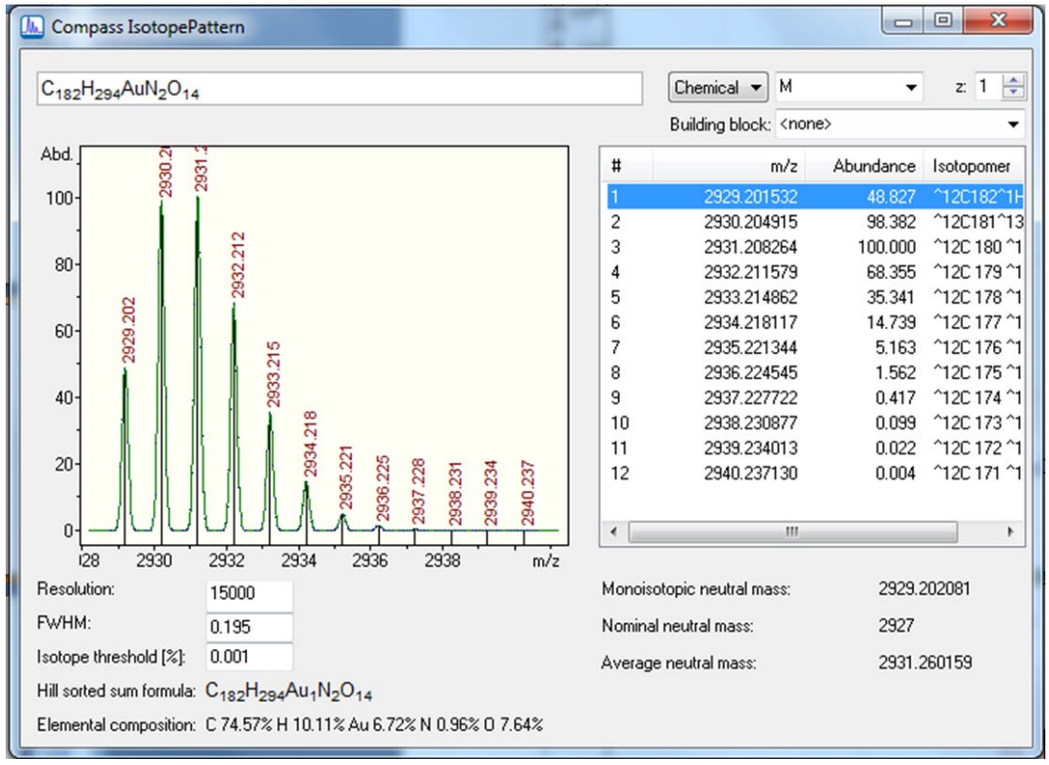

Figure S17. Up, MALDI-TOF (positive m/z) spectrum of **4**. Red with DIT (dithranol) as matrix; Blue with DCTB (trans-2-[3-(4-tert-Butylphenyl)-2-methyl-2-propenylidene]malononitrile) as matrix. Down, simulated isotopic pattern for $[M - BF_4]^+$.

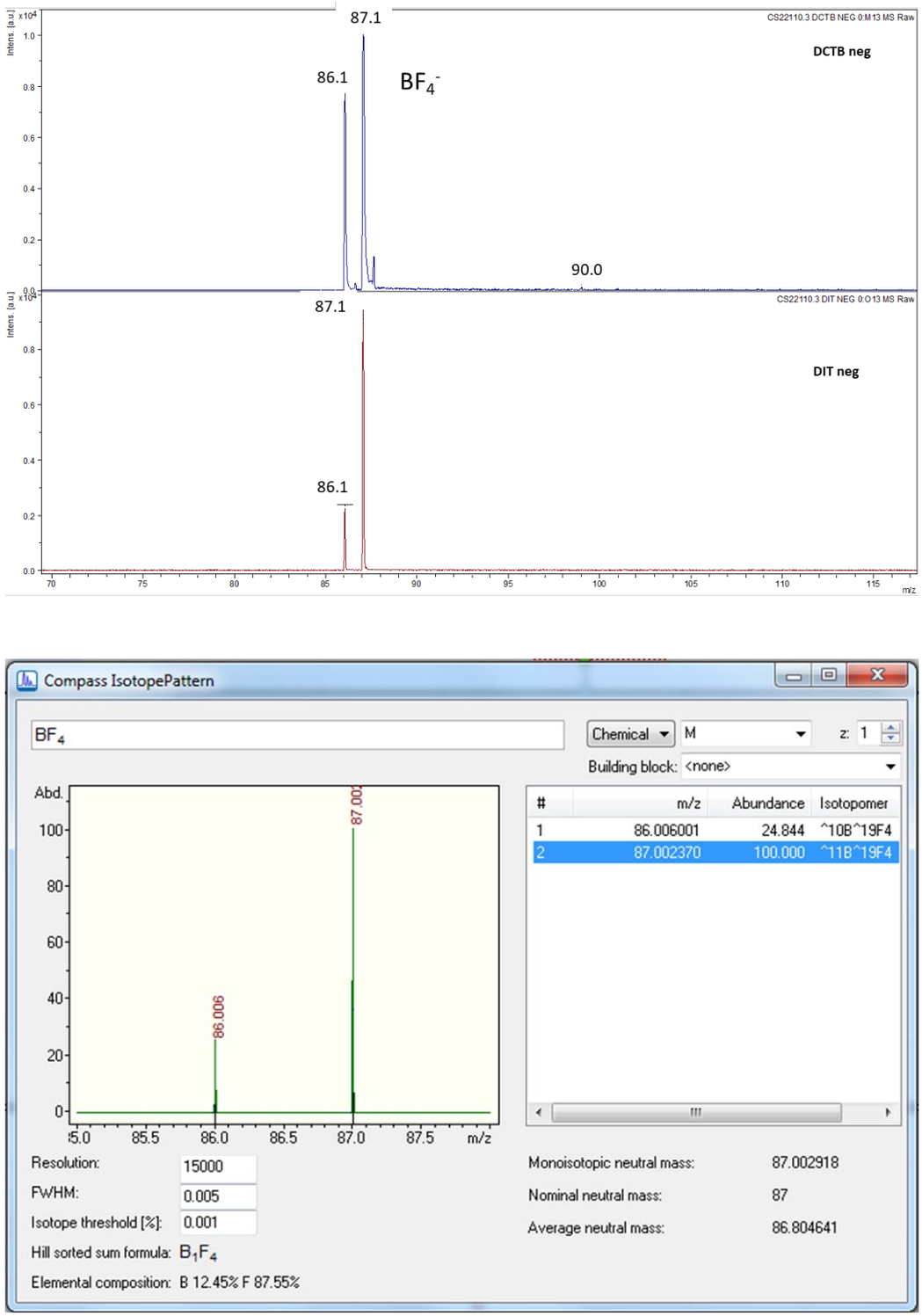

Figure S18. Up, MALDI-TOF (negative m/z) spectrum of **4**. Red with DIT (dithranol) as matrix; Blue with DCTB (trans-2-[3-(4-tert-Butylphenyl)-2-methyl-2-propenylidene]malononitrile) as matrix. Down, simulated isotopic pattern for BF_4^-.

Fluorescence lifetimes

Fluorescence decays in dichloromethane, at room temperature. Lifetimes were obtained with the Time Correlated Single Photon Counting (TCSPC) and MCP-PMT counter module (TCC2) of the FLS980 spectrometer. Fluorescence decays were analyzed with the method of non-linear least squares iterative deconvolution and the quality of the fits was judged by the values of the reduced Chi-square (c2) and the autocorrelation function of the residuals using the FAST (Advanced Fluorescence Lifetime Analysis Software) program provided by the equipment.

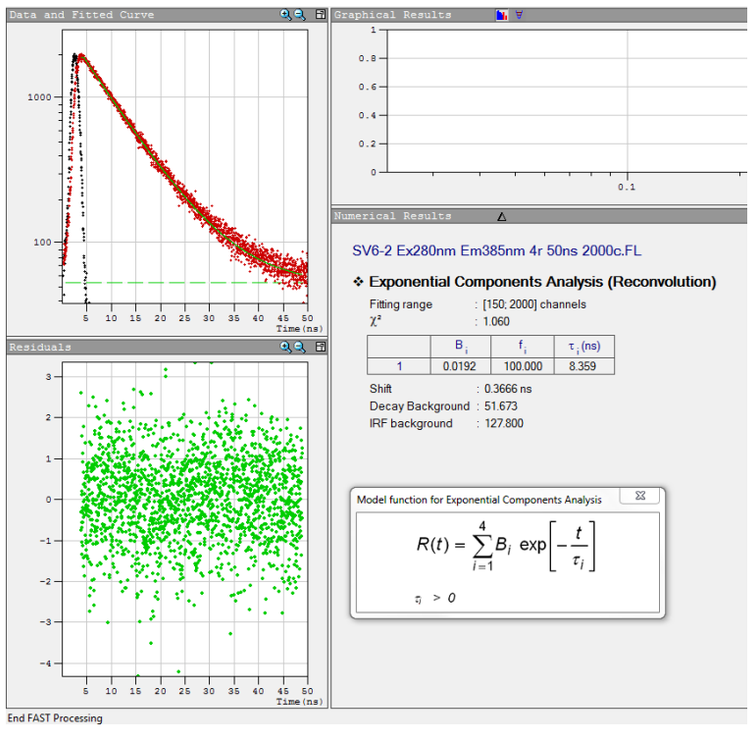

Figure S19. Fluorescence decay for **$CNC_6H_4OC_6H_{12}O$-TPh**. Measurement Conditions: EPL280, MCP-PMT λex = 280 nm, Δλem = 4 nm, pulse 50 ns 2000c λem = 385nm

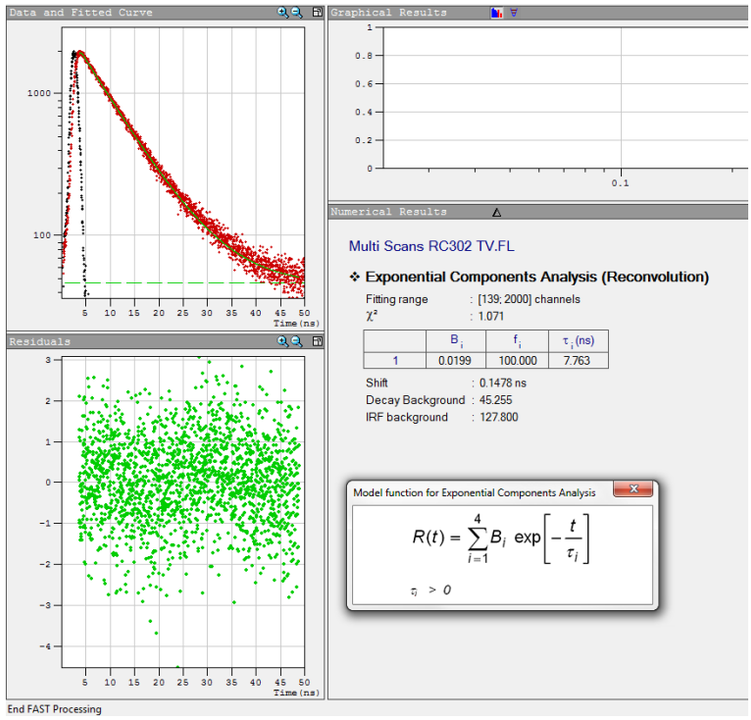

Figure S20. Fluorescence decay for **1**. Measurement Conditions: EPL280, MCP-PMT λex = 280 nm, Δλem = 4 nm, pulse 50 ns 2000c λem = 385nm.

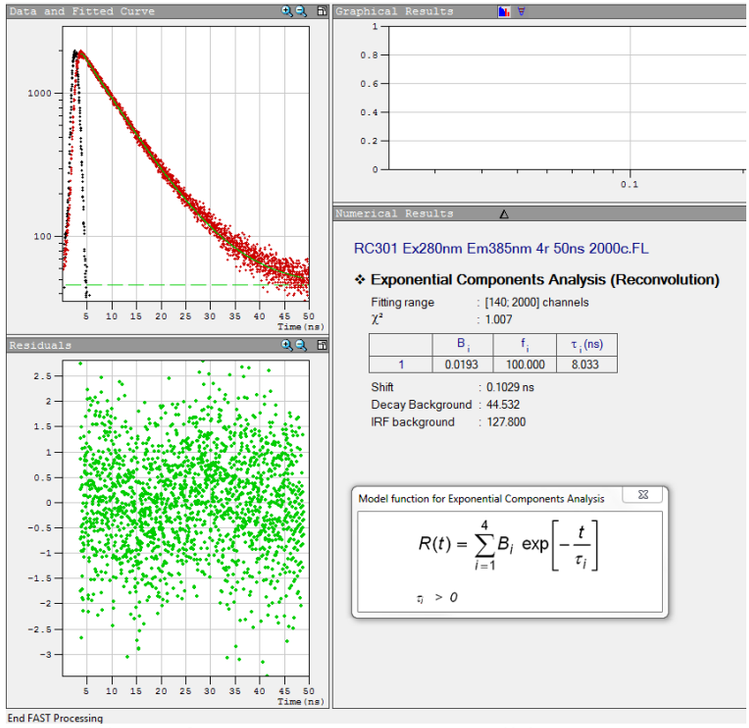

Figure S21. Fluorescence decay for **2**. Measurement Conditions: EPL280, MCP-PMT λex = 280 nm, Δλem = 4 nm, pulse 50 ns 2000c λem = 385nm.

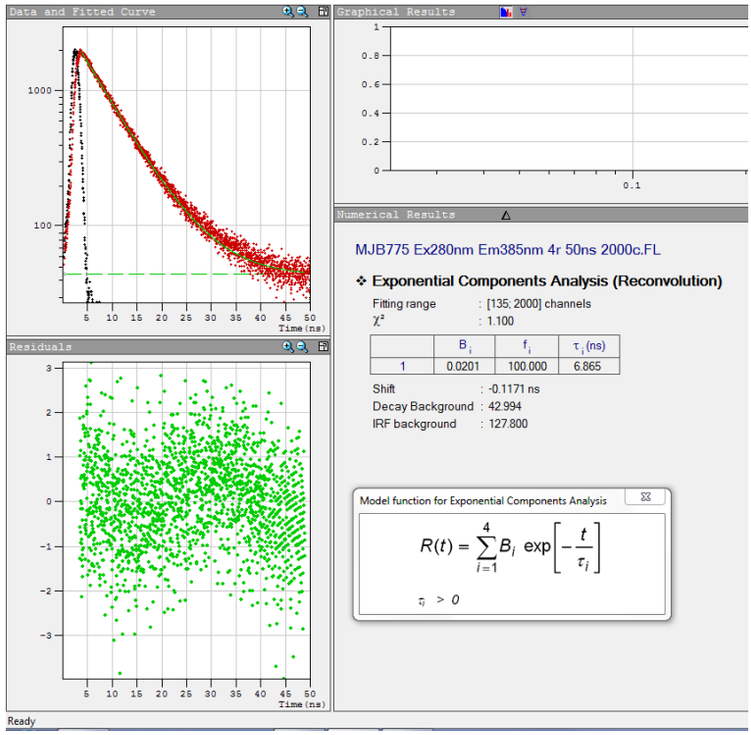

Figure S22. Fluorescence decay for **3**. Measurement Conditions: EPL280, MCP-PMT λex = 280 nm, Δλem = 4 nm, pulse 50 ns 2000c λem = 385nm.

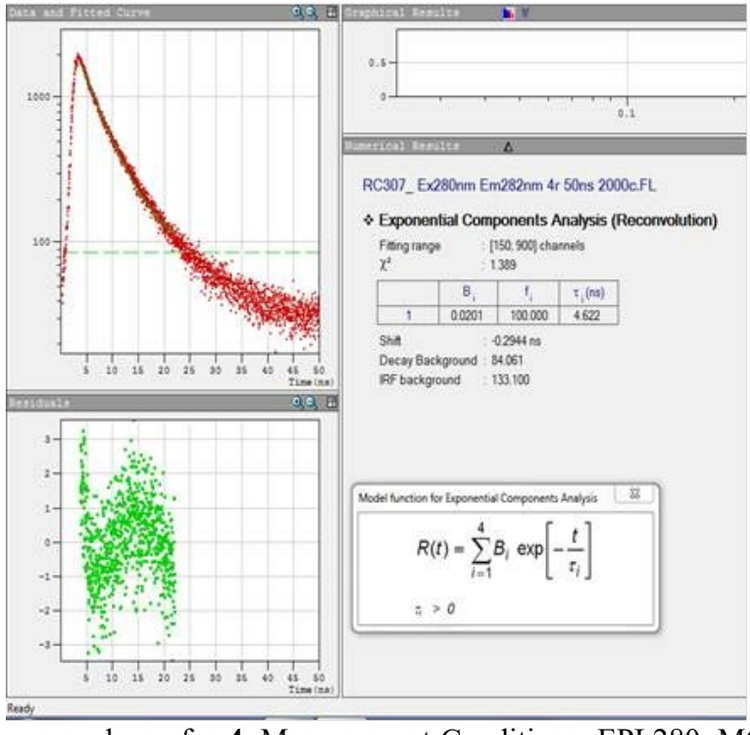

Figure S23. Fluorescence decay for **4**. Measurement Conditions: EPL280, MCP-PMT λex = 280 nm, Δλem = 4 nm, pulse 50 ns 2000c λem = 382nm.

DSC scans: a) first heating, b) first cooling, c) second heating.

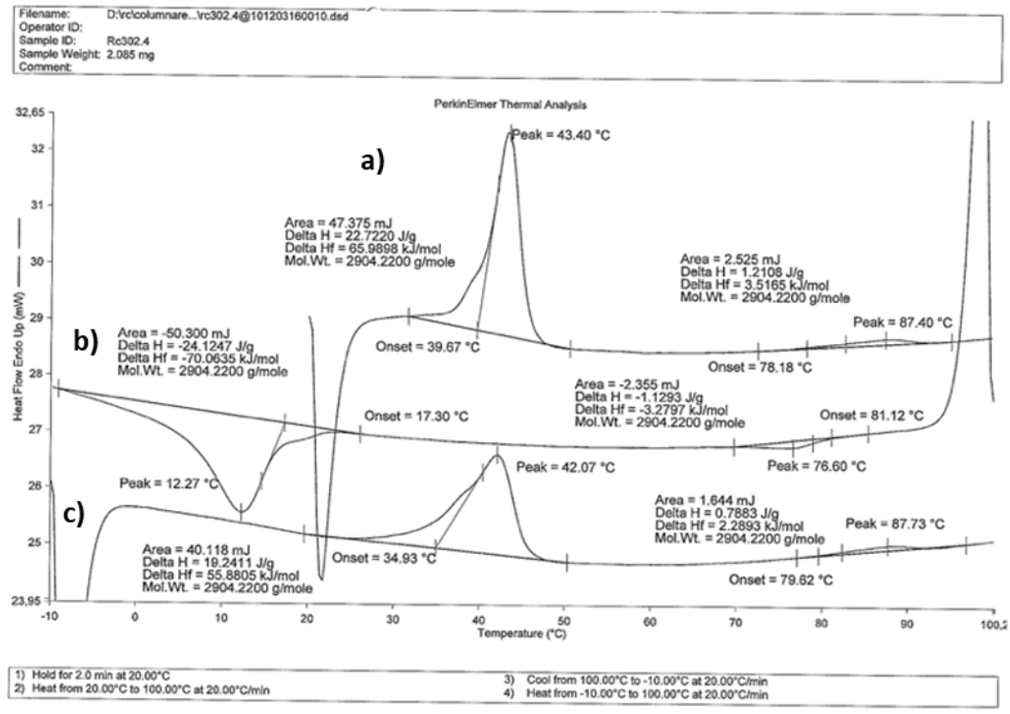

Figure S24. DSC scans of **1**

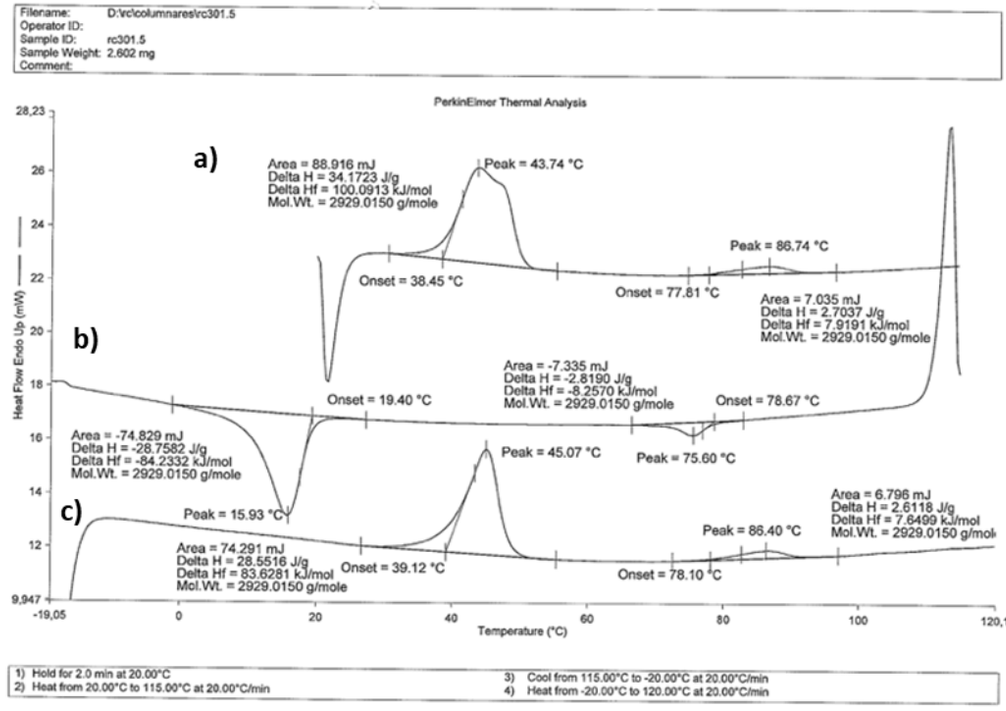

Figure S25. DSC scans of **2**

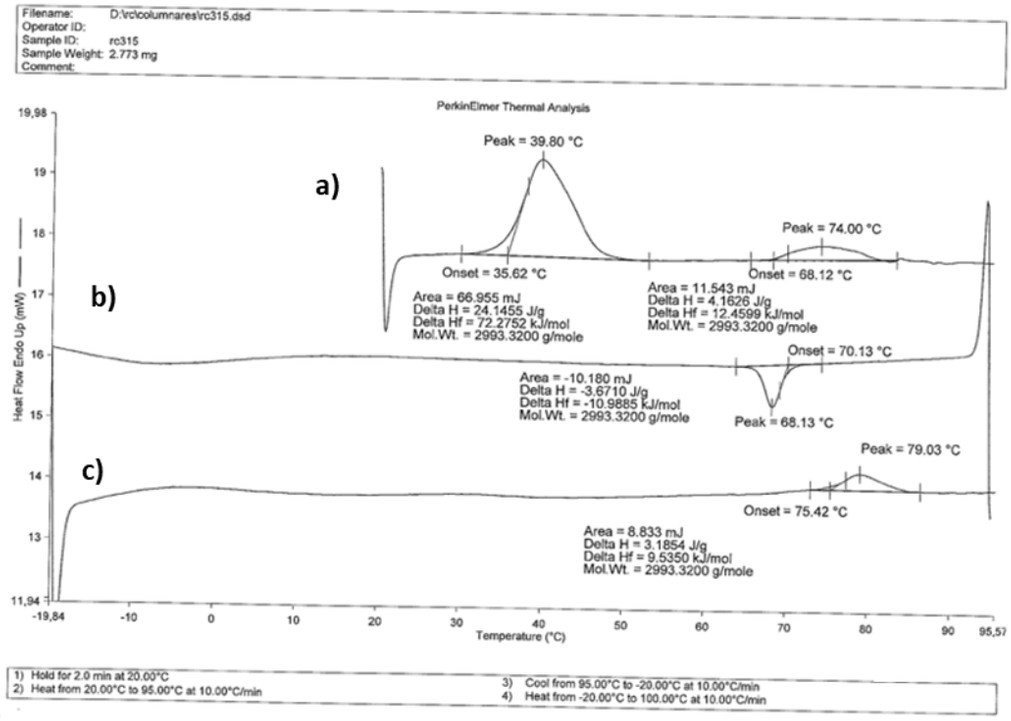

Figure S26. DSC scans of **3**

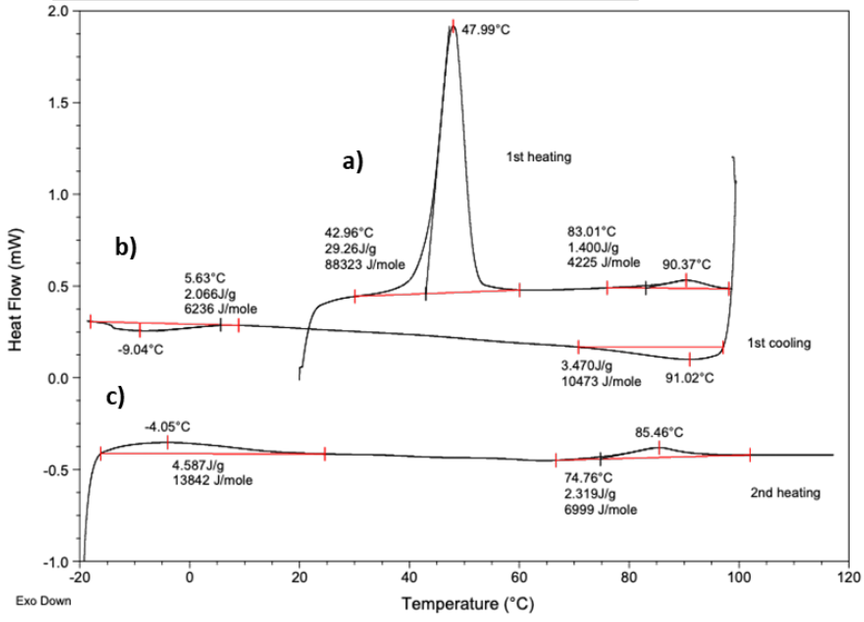

Figure S27. DSC scans of **4**

Thermogravimetric analysis

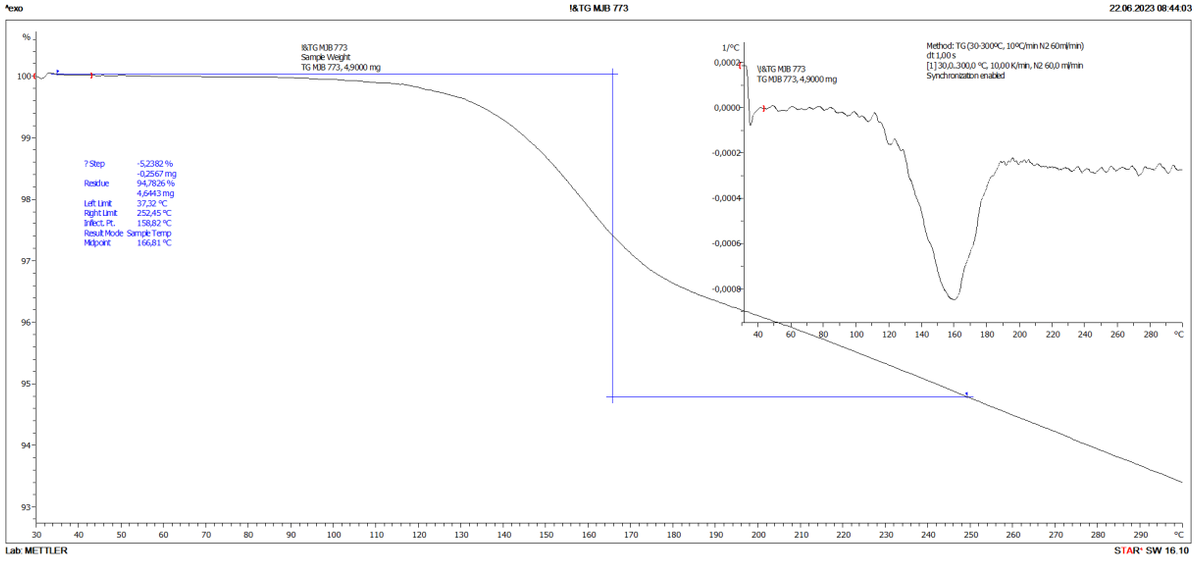

Figure S28. TGA scan of **1**

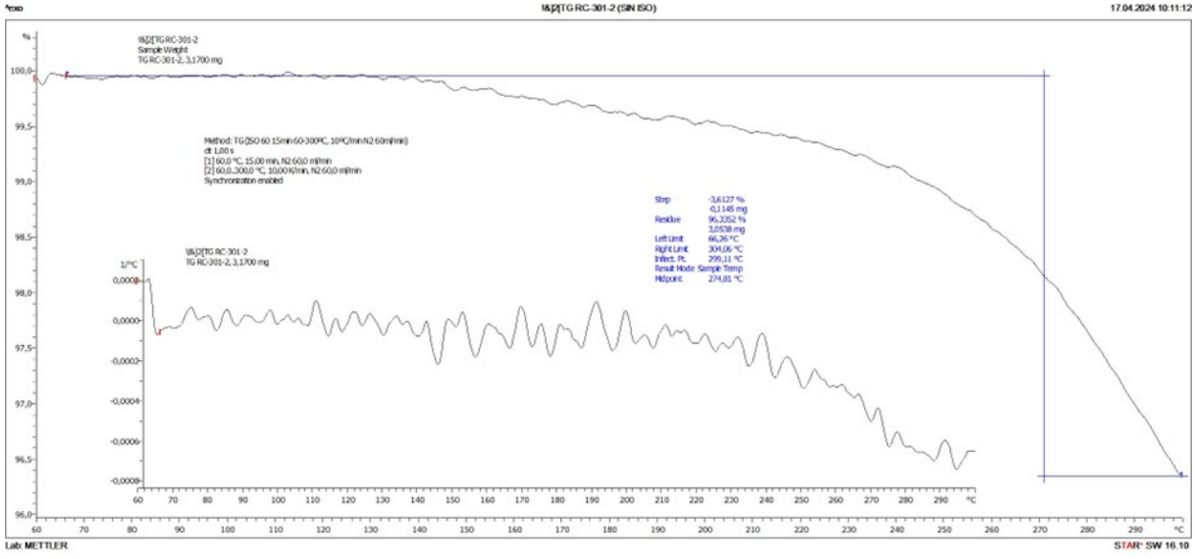

Figure S29. TGA scan of **2**

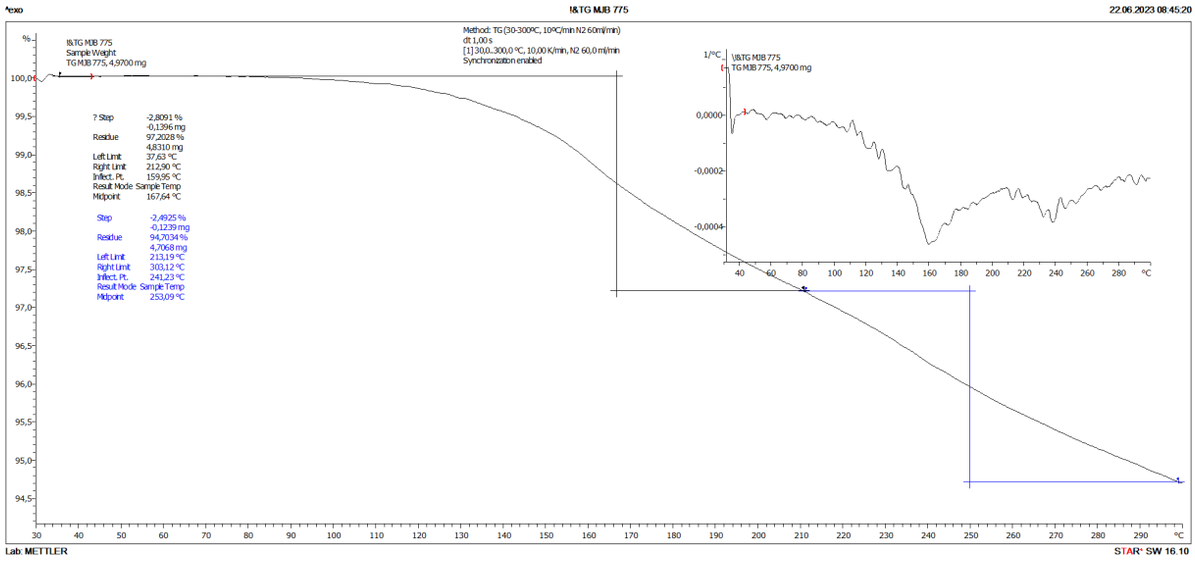

Figure S30. TGA scan of **3**

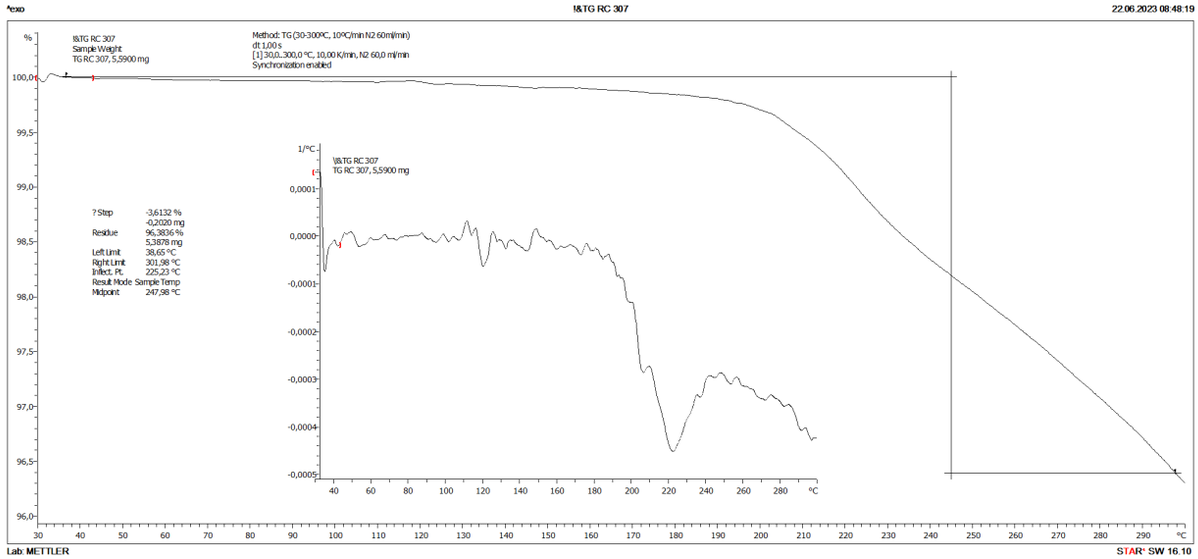

Figure S31. TGA scan of **4**

S/WAXS

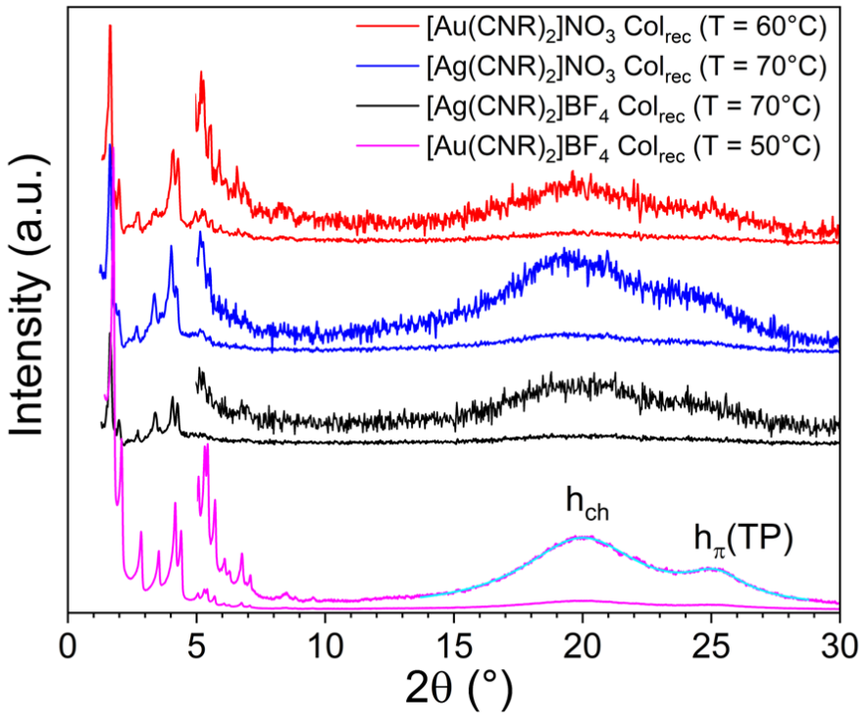

Figure S32. S/WAXS profiles of the four complexes.

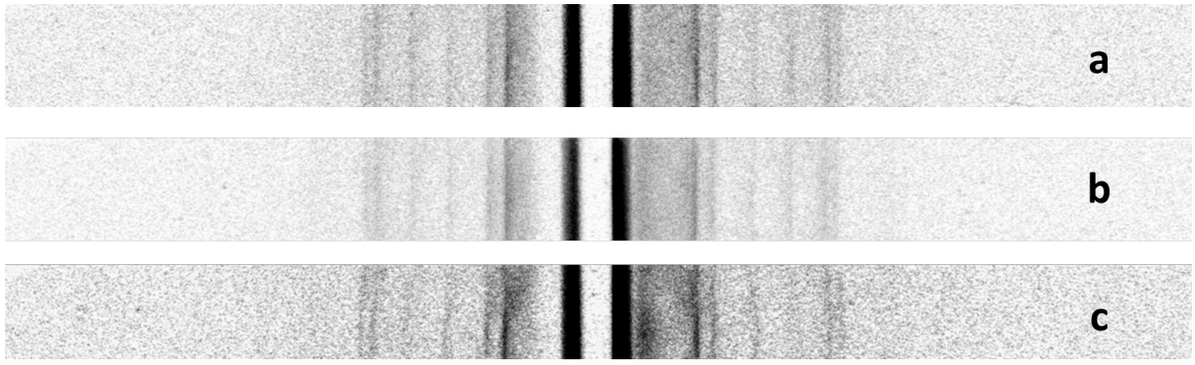

Figure S33. S/WAXS (Image plate) of complexes a) $[Ag(CNR)_2](BF_4)$ at 70°C, b) $[Ag(CNR)_2](NO_3)$ at 70°C, and c) $[Au(CNR)_2](NO_3)$ at 60°C.

Table S1. Mesophases indexation parameters.

Compound T/ºC		d_{meas}/Å[a]	*hk*[b]	I[c]	d_{calc}/Å[a]	Parameters[ds]
1	1.679	52.57	11	VS (sh)	-	Col_{rec}-*c*2*mm*
$[Ag(CNR)_2](NO_3)$	1.994	44.27	20	S (sh)	-	a = 88.54 Å
70	2.708	32.60	02	M (sh)	32.66	b = 65.33 Å
	3.367	26.22	22	M (sh)	26.28	S = 5784.42 Å^2
	3.987	22.14	40	M (sh)	22.13	
	4.180	21.12	13	M (sh)	21.15	
	5.172	17.07	51	W (sh)	17.09	
	19.39	4.57	h_{ch}	VS (br)	-	
	24.79	3.59	h_{π}	S (br)	-	
2	1.664	53.04	11	VS (sh)	-	Col_{rec}-*c*2*mm*
$[Ag(CNR)_2](BF_4)$	1.983	44.51	20	S (sh)	-	a = 89.02 Å
70	2.675	33.00	02	M (sh)	33.02	b = 66.04 Å
	3.335	26.47	22	M (sh)	26.52	S = 5879.12 Å^2
	3.984	22.16	40	M (sh)	22.25	
	4.145	21.30	13	M (sh)	21.36	
	19.85	4.47	h_{ch}	VS (br)	-	
	25.31	3.52	h_{π}	S (br)	-	
3	1.667	52.95	11	VS (sh)	-	Col_{rec}-*c*2*mm*
$[Au(CNR)_2](NO_3)$	2.012	43.87	20	S (sh)	-	a = 87.74 Å
60	2.658	33.21	02	M (sh)	33.20	b = 66.40 Å
	3.340	26.43	22	M (sh)	26.47	S = 5826.43 Å^2
	4.025	21.93	40	M (sh)	21.93	
	4.128	21.39	13	M (sh)	21.46	
	5.02	17.59	33	M (sh)	17.65	
	5.23	16.88	51	M (sh)	16.96	
	5.32	16.60	04	M (sh)	16.60	
	5.67	15.56	24	W (sh)	15.53	
	5.96	14.82	60	W (sh)	14.62	
	6.64	13.30	62/44	W (sh)	13.38/13.24	
	20.14	4.40	h_{ch}	VS (br)	-	
	25.2	3.53	h_{π}	S (br)	-	
4	1.758	50.21	11	VS (sh)	-	Col_{rec}-*c*2*mm*
$[Au(CNR)_2](BF_4)$	2.081	42.42	20	S (sh)	-	a = 84.84 Å
70	2.840	31.08	02	M (sh)	31.14	b = 62.29 Å
	3.519	25.09	22	M (sh)	25.10	S = 5284.68 Å^2

	4.159	21.23	40	M (sh)	21.21	
	4.377	20.17	13	M (sh)	20.17	
	5.046	17.50	42	M (sh)	17.53	
	5.271	16.75	33	M (sh)	16.74	
	5.392	16.37	51	M (sh)	16.37	
	5.67	15.57	04	W (sh)	15.57	
	6.08	14.52	24	W (sh)	14.62	
	6.27	14.08	60	W (sh)	14.14	
	6.72	13.14	53	VW (sh)	13.14	
	7.04	12.54	44	VW (sh)	12.55	
	7.42	11.90	71	VW (sh)	11.89	
	8.51	10.38	06	VW (sh)	10.38	
	9.50	9.30	46/91	VW (sh)	9.32	
	19.78	4.48	h_{ch}	S (br)	-	
	24.90	3.57	h_{π}	S (br)	-	

Capacitance vs frequency (*C*' vs *f*) plots

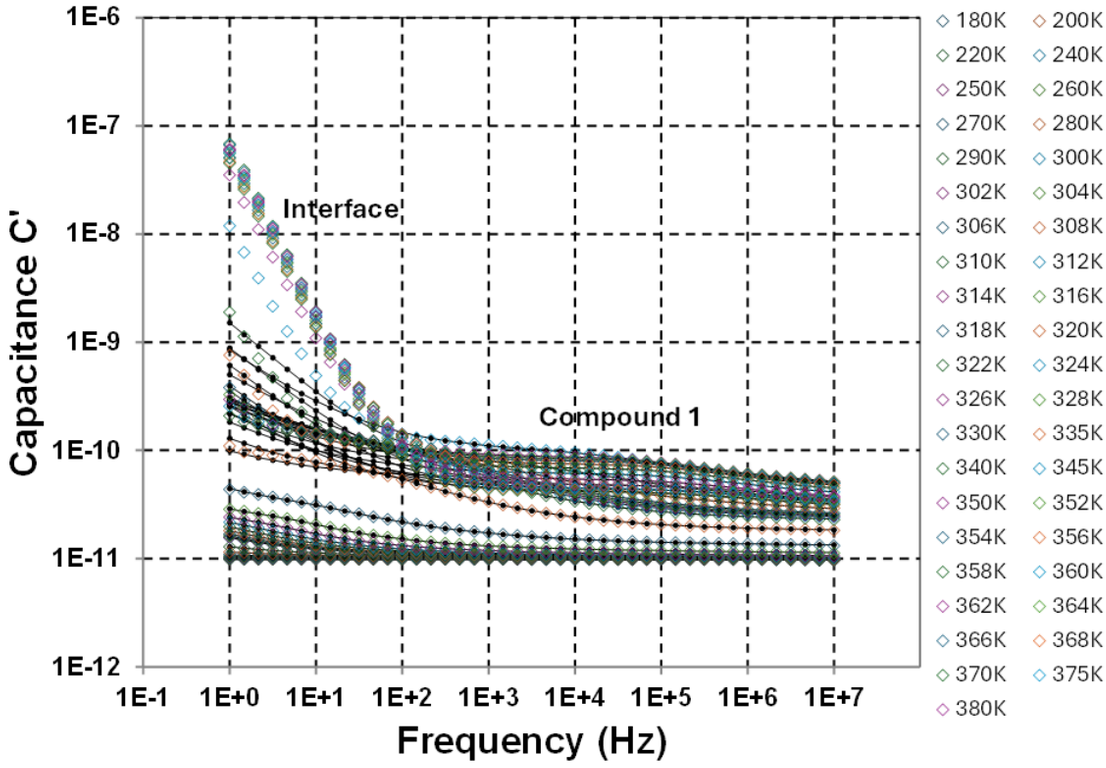

Figure S34. Capacitance vs frequency (*C*' vs *f*) plots on double-logarithmic axes for Compound **1**. The linear increase of *C*' at the low-*f* end is another hallmark feature of ionic conductivity. The equivalent plots for all other compounds show very similar features.

References

[1] R. A. Velapoldi and H. H. Tønnesen, *Journal of Fluorescence*, **2004**, *14*, 465−472.

[2] C. Cuerva, J. A. Campo, M. Cano, J. Sanz, I. Sobrados, V. Diez-Gómez, A. Rivera-Calzada, R. Schmidt, *Inorg. Chem.,* 2016, **55**, 6995−7002

[3] R. Chico, E. de Domingo, C. Domínguez, B. Donnio, B. Heinrich, R. Termine, A. Golemme, S. Coco and P. Espinet,, *Chem. Mater*. 2017, **29**, 7587−7595

[4] R. Uson, A. Laguna, M. Laguna, *Inorg. Synth.*, 1989, **26,** 85−91.